

# Algorithms for entanglement renormalization

G. Vidal<sup>1</sup>

<sup>1</sup>*School of Physical Sciences, the University of Queensland, QLD 4072, Australia*

(Dated: November 3, 2021)

We discuss three algorithms for the simulation of quantum many-body systems on a lattice using the multi-scale entanglement renormalization ansatz (MERA). The cost of simulating a system on a lattice with  $N$  sites scales as  $O(N)$  and decreases to  $O(\log(N))$  when the system is invariant under translations. We also describe several strategies to address linear and quadratic optimizations over a set of isometric tensors.

PACS numbers:

## I. INTRODUCTION

Entanglement renormalization [1] is a local reorganization of the Hilbert space of a quantum many-body system that aims to reduce the amount of entanglement in its wave function. It was introduced to address a major computational obstacle in real space renormalization group (RG) methods [2], responsible for limitations in their performance and range of applicability, namely the proliferation of degrees of freedom that occurs under successive applications of a RG transformation.

Entanglement renormalization is built around the assumption that, as a result of the local character of physical interactions, some of the relevant degrees of freedom in the ground state of a many-body system can be decoupled from the rest by unitarily transforming small regions of space. Accordingly, unitary transformations known as *disentangler*s are applied locally to the system in order to identify and decouple such degrees of freedom, which are then safely removed and therefore do no longer appear in any subsequent coarse-grained description. This prevents the harmful accumulation of degrees of freedom and thus leads to a sustainable real space RG transformation, able to explore lattice systems with tens of thousands of sites, even at a quantum critical point. It also leads to the *multi-scale entanglement renormalization ansatz* (MERA), a variational ansatz for many-body states [3].

The MERA, based on a class of quantum circuits, is particularly successful at describing quantum critical ground states on a lattice [1, 4] and it is also naturally suited for systems with topological order [5]. From the computational viewpoint, the key property of the MERA is that it can be manipulated efficiently — leading to an efficient evaluation of expectation values for local observables and two-point correlators. This is due to the causal structure of the underlying quantum circuit, as explained in Ref. [3], where we also indicated how the MERA can be used to efficiently simulate a time evolution and (through evolution in imaginary time) compute ground states.

In this manuscript we describe several algorithms based on the MERA, thereby spelling out the details of a number of results previously announced or sketched in Refs. [1, 3]. More specifically, we present the following

three algorithms:

Sect.IV: *RG transformation for Hamiltonians.* Computation of a MERA for the low energy subspace of a local Hamiltonian.

Sect.V: *RG transformation for states.* Computation of a MERA from another tensor network representation.

Sect.VI: *Hybrid algorithm.* Computation of a MERA for the ground state and low energy excitations of a local Hamiltonian, with the help of an auxiliary algorithm.

[See also Ref. [23] for an algorithm to simulate time evolution with the MERA.]

A highlight of the algorithms is that they can address a quantum many-body system on a lattice of  $N$  sites with a cost that scales only as  $O(N)$  and that, when the system is invariant under translations, drops to  $O(\log(N))$ . We envisage that these algorithms will facilitate substantially the study of collective quantum phenomena in  $D$  spatial dimensions, including quantum criticality and topological order.

A major technical difficulty in implementing the above algorithms is that they involve linear and quadratic optimizations over sets of isometric tensors, for which no exact solutions are known. Thus, in preparation for such tasks, we first describe the classes of optimizations that will be required and present a small tool box of strategies to address them. Most of these strategies can be used in the optimization of arbitrary quantum circuits and may find applications beyond the MERA algorithms.

We emphasize that in these notes we neither provide evidence of the performance of the algorithms nor discuss their applications. Instead, we focus merely on describing the algorithms. This is done in a relatively self-contained manner and with a level of detail that, hopefully, provides the interested reader with enough information to implement the algorithms. We refer to [1, 3, 4] for additional theoretical background and benchmark calculations. Much work in progress is based on the algorithms presented here.

The paper is organized as follows. In section II we introduce the MERA and review some background material. Sect. III is devoted to optimizations involving

isometric transformations. Then in Sects. IV to VI we present the algorithms based on the MERA. Finally, Sect. VII contains some additional remarks and conclusions.

## II. QUANTUM CIRCUITS, ISOMETRIC TRANSFORMATIONS AND THE MERA

In this section we review some background material and establish the notation to be used throughout the rest of the manuscript.

### A. Efficient simulation.

This paper is concerned with the efficient simulation of quantum many-body systems defined on a lattice. We consider a lattice  $\mathcal{L}$  made of  $N$  sites, where each site  $s \in \mathcal{L}$  is described by a complex vector space  $\mathbb{V}$  of finite dimension  $\chi$ . A state of the many-body system is thus represented by a vector  $|\Psi\rangle \in \mathbb{V}^{\otimes N}$ . This vector can be expanded in a local basis,

$$|\Psi\rangle = \sum_{i_1 i_2 \dots i_N=1}^{\chi} c_{i_1 i_2 \dots i_N} |i_1\rangle |i_2\rangle \dots |i_N\rangle \quad (1)$$

by specifying  $\chi^N$  complex coefficients  $c_{i_1 i_2 \dots i_N}$ . That is,  $|\Psi\rangle$  depends on a number of coefficients that grows exponentially with the size  $N$  of the lattice. As a result, simulating a large system by keeping a list with all these coefficients is computationally unaffordable.

Addressing large systems may still be at hand if all the states  $|\Psi\rangle$  of interest form a reasonably small subset of  $\mathbb{V}^{\otimes N}$ . In that case, here is a user guide to simulating large systems:

(i) Find an *efficient representation* of the states  $|\Psi\rangle$  in this subset, that is, a way of specifying  $|\Psi\rangle$  by using just  $\text{poly}(N)$  parameters. Not all efficient representations are equally useful. We need an efficient representations from which relevant information about  $|\Psi\rangle$ , such as the expectation value of local observables, can be efficiently extracted.

(ii) Find an *efficient algorithm* to compute the state  $|\Psi\rangle$  for the specific problem under consideration. For instance, given a local Hamiltonian  $H$  defined on lattice  $\mathcal{L}$ , we may want to study its ground state  $|\Psi_{gr}\rangle$  or a time evolution  $|\Psi(t)\rangle \equiv e^{-iHt}|\Psi(0)\rangle$ . Assuming that an efficient representation for  $|\Psi_{gr}\rangle$  or  $|\Psi_t\rangle$  exists, we will still need this algorithm to find it.

The MERA offers an efficient representation of a subset of states  $|\Psi\rangle \in \mathbb{V}^{\otimes N}$  from which the expectation value of local observables can be computed also efficiently [3]. In addition, assuming that all the relevant states can be represented by a MERA, it is possible to compute the ground state  $|\Psi_{gr}\rangle$  from  $H$ ; and the evolved state  $|\Psi(t)\rangle$  from  $H$  and a MERA for the initial state  $|\Psi(0)\rangle$ . Sections IV to ?? of this paper are precisely devoted to describing algorithms to efficiently accomplish these tasks. In

preparation for them, the rest of this section introduces the MERA and reviews some of its main properties.

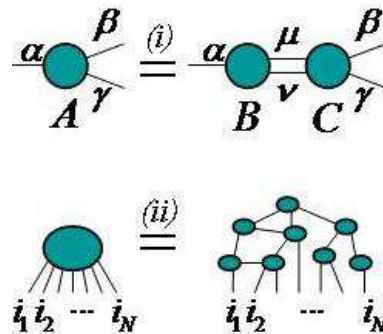


FIG. 1: (i) Throughout the paper we use a diagrammatic representation of tensors and tensor multiplications. The example represents a tensor  $A$  that results from multiplying tensors  $B$  and  $C$  according to  $A_{\alpha\beta\gamma} = \sum_{\mu\nu} B_{\alpha\mu\nu} C_{\mu\nu\beta\gamma}$ . (ii) A tensor network (right) is used to specify a tensor (left) with the  $\chi^N$  coefficients  $c_{i_1 i_2 \dots i_N}$  of a state  $|\Psi\rangle \in \mathbb{V}^{\otimes N}$ , Eq. (1).

### B. Tensor network and quantum circuit representations of a quantum many-body state.

A *tensor network* representation for state  $|\Psi\rangle$  is an encoding of the  $\chi^N$  coefficients of Eq. (1) in terms of a collection of tensors that are interconnected into a network, see Fig. (1).

We are interested in the case where the tensor network leads to an efficient way of specifying  $|\Psi\rangle$ . This occurs, for instance, when both the number and size of tensors in the network are allowed to grow at most polynomially with  $N$ . In addition, we would like to efficiently extract information about  $|\Psi\rangle$  from the representation. This can be achieved e.g. by contracting the tensor network, but such contractions are only efficient for a restricted class of networks [6].

Examples of efficient tensor network representations used to simulate many-body systems are the matrix product state (MPS) [7], tree tensor networks (TTN) [8] and the projected entangled pair state (PEPS) [9].

A *quantum circuit* representation is a particular class of tensor network representation. We can think of a quantum circuit as a collection of tensors or *gates* that are interconnected by wires into a network on which a discrete time variable  $\Theta$  can be defined, see Fig. (2). In addition, each gate  $u$  is constrained to be a unitary transformation between the spaces  $\mathbb{V}_{in}$  and  $\mathbb{V}_{out}$  of its incoming and outgoing wires,

$$u^\dagger u = I_{in}, \quad uu^\dagger = I_{out}. \quad (2)$$

Let us assume that the circuit has  $N$  incoming and  $N$  outgoing wires and  $\text{poly}(N)$  gates, and that each wire is described by a complex vector space  $\mathbb{V}$  of finite dimension

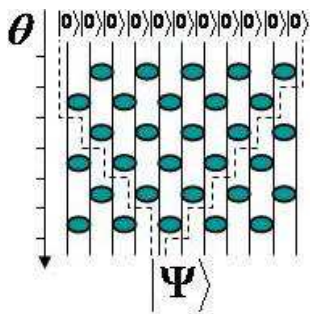


FIG. 2: Quantum circuit representation of state  $|\Psi\rangle \in V^{\otimes N}$ . This state of our lattice  $\mathcal{L}$  can be efficiently specified by describing the poly( $N$ ) gates of the circuit. Notice that the causal cone of the 5th outgoing wire (discontinuous line) expands back in time and its width becomes of order  $O(N)$ .

$\chi$ , so that the circuit implements a unitary transformation  $U : \mathbb{V}^{\otimes N} \rightarrow \mathbb{V}^{\otimes N}$ . Then  $U$  transforms an initial product state  $|0\rangle^{\otimes N}$  into an entangled state  $|\Psi\rangle \in \mathbb{V}^{\otimes N}$ ,

$$|\Psi\rangle = U|0\rangle^{\otimes N} = \sum_{i_1 i_2 \dots i_n} U_{0 \dots 0}^{i_1 i_2 \dots i_n} |i_1\rangle |i_2\rangle \dots |i_n\rangle. \quad (3)$$

Therefore another way to efficiently specify some states  $|\Psi\rangle$  of lattice  $\mathcal{L}$  is in terms of a quantum circuit together with an unentangled input state, say  $|0\rangle^{\otimes N}$ , see Fig (2).

Notice, however, that a quantum circuit representation is still not very useful in general, because we do not know how to efficiently compute e.g. the expectation value of local observables. [Otherwise we would be able to simulate a quantum computer!] This last fact can be related to how information propagates in the circuit, where the causal cone of an outgoing wire spreads back in time to quickly cover all the incoming wires, see Fig. (2). As we discuss below, the MERA turns out to correspond to a particular class of circuit, see Fig. (3), where the causal cone of each outgoing wire has bounded width. Thanks to this feature, local expectation values can be computed efficiently.

Before we introduce the MERA, it is convenient to generalize the unitary quantum circuit to allow for *isometric* gates  $w$ . A gate  $w : \mathbb{V}_{in} \rightarrow \mathbb{V}_{out}$ , where the dimensions  $d_{in}$  and  $d_{out}$  for the input and output spaces fulfill  $d_{in} \leq d_{out}$ , is isometric if

$$w^\dagger w = I_{in}. \quad (4)$$

An *isometric quantum circuit* is then a quantum circuit where each gate is an isometric tensor. In particular, the circuit itself corresponds to an isometric transformation  $U$ ,

$$U : \mathbb{V}^{\otimes M} \rightarrow \mathbb{V}^{\otimes N}, \quad U^\dagger U = I, \quad (5)$$

between  $M$  incoming wires and  $N$  outgoing wires. Accordingly, if  $M = 0$ , the (rank 1) isometric transformation  $U$  efficiently specifies a vector  $|\Psi\rangle \in \mathbb{V}^{\otimes N}$  of our

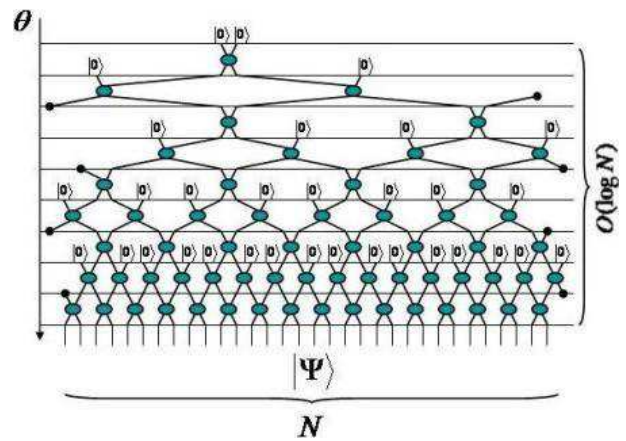


FIG. 3: Example of quantum circuit corresponding to the MERA (for a one-dimensional lattice  $\mathcal{L}$ ). The  $N$  incoming quantum wires are progressively introduced throughout the  $O(\log(N))$  rows of gates in the circuit. Notice that the some of the wires are connected through the boundaries.

lattice  $\mathcal{L}$ , whereas when  $M \geq 1$ ,  $U$  can be used to specify a subspace of dimension  $\chi^M$  within  $\mathbb{V}^{\otimes N}$ .

Two classes of tensor networks used to represent quantum many-body systems, namely MPS [7] and TTN [8], can be reexpressed as isometric quantum circuits.

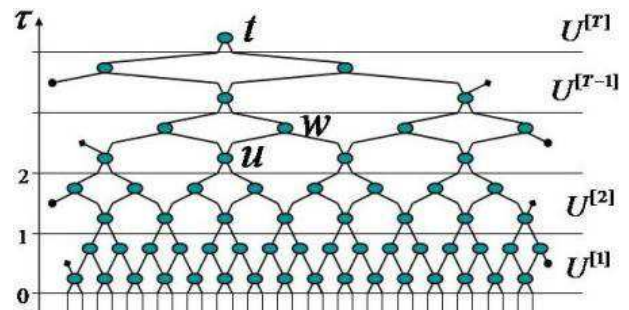


FIG. 4: MERA for the state  $|\Psi\rangle$  of a lattice  $\mathcal{L}$  in one spatial dimension, as codified in an isometric transformation  $U \in \mathcal{M}$  that decomposes into  $T$  layers, each one represented by an isometric transformation  $U^{[\tau]}$ . Whereas most layers further decompose into a row of disentanglers  $u$  and a row of isometries  $w$ , the top layer  $U^{[T]}$  consists of only a vector tensor  $t$ .

### C. The MERA.

The *multi-scale entanglement renormalization ansatz* (MERA) can be described in terms of an isometric quantum circuit with  $N$  outgoing wires, such as that in Fig. (4). The circuit is organized into  $T \equiv \log(N)$  layers, labeled by an index  $\tau$ ,  $1 \leq \tau \leq T$ , that grows for decreasing values of the time  $\Theta$ . Each layer  $\tau$  corresponds to a subcircuit implementing an isometric transformation  $U^{[\tau]}$ , in terms of which an overall isometric transformation  $U$

reads

$$U = U^{[1]}U^{[2]} \dots U^{[T]}. \quad (6)$$

We write  $U \in \mathcal{M}$  to express the fact that  $U$  has the circuit structure of the MERA.

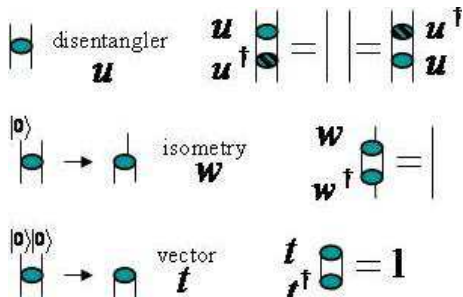


FIG. 5: The MERA contains three types of gates: disentanglers  $u$ , isometries  $w$  and normalized vectors  $t$ . The figure shows how an isometry  $w$  and a vector  $t$  can be understood as unitary gates in which several of the incoming wires have a fixed state  $|0\rangle$ .

Each transformation  $U^{[\tau]}$  can be further decomposed into several isometric tensors. Depending on the dimensions  $d_{in}$  and  $d_{out}$  for their input and output spaces, we distinguish three classes of tensors, as represented in Fig. (5): (i) when  $d_{in} = d_{out}$  the tensor is unitary and we call it a *disentangler*, denoted  $u$ ; (ii) when  $d_{in} = 1$  the tensor is a normalized vector  $t$  in  $\mathbb{V}_{out}$ ; (iii) in the rest of cases,  $1 < d_{in} < d_{out}$ , we refer to the tensor  $w$  as an *isometry*. A typical  $U^{[\tau]}$  is made of a row of disentanglers  $u^{[\tau,s]}$  and a row of isometries  $w^{[\tau,s]}$ , where we use label  $s$  (corresponding to a site in  $\mathcal{L}_\tau$ ) to identify tensors within  $U^{[\tau]}$ , see Fig. (6).

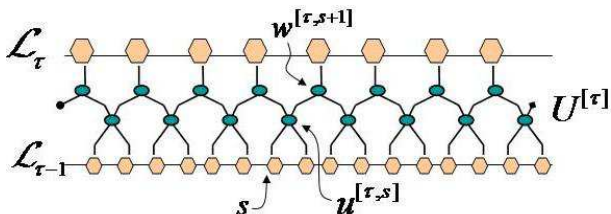


FIG. 6: The one-layer isometric transformation  $U^{[\tau]}$  can be used to define lattice  $\mathcal{L}_\tau$  in terms of lattice  $\mathcal{L}_{\tau-1}$ . When applied to a state  $|\Psi_{\tau-1}\rangle$  in  $\mathcal{L}_{\tau-1}$ , it produces a coarse-grained state  $|\Psi_\tau\rangle \equiv U^{[\tau]\dagger}|\Psi_{\tau-1}\rangle$ . Similarly, we can define an effective local Hamiltonian  $H_\tau \equiv U^{[\tau]\dagger}H_{\tau-1}U^{[\tau]}$  for  $\mathcal{L}_\tau$  in terms of a local Hamiltonian  $H_{\tau-1}$  for  $\mathcal{L}_{\tau-1}$ .

The isometric transformation  $U^{[1]}$  can be used to define a lattice  $\mathcal{L}_1$  from the original lattice  $\mathcal{L}_0 \equiv \mathcal{L}$ . Similarly, if  $H_0 \equiv H$  and  $|\Psi_0\rangle \equiv |\Psi\rangle$  are the Hamiltonian and vectors of out lattice  $\mathcal{L}$ , we can use the  $U^{[1]}$  to define in  $\mathcal{L}_1$  both an effective Hamiltonian  $H_1$  and coarse-grained state  $|\Psi_1\rangle$ . More generally,  $U^{[\tau]}$  allows us to define lattice  $\mathcal{L}_\tau$ , Hamiltonian  $H_\tau$  and state  $|\Psi_\tau\rangle$

from  $\mathcal{L}_{\tau-1}$ ,  $H_{\tau-1}$  and  $|\Psi_{\tau-1}\rangle$ , see Fig. (6). Notice that the incoming and outgoing wires of  $U^{[\tau]}$  are identified with the sites of lattices  $\mathcal{L}_{\tau-1}$  and  $\mathcal{L}_\tau$  respectively. By iteration we obtain a series of increasingly coarse-grained lattices  $\{\mathcal{L}_0, \mathcal{L}_1, \dots, \mathcal{L}_{T-1}\}$  and corresponding effective Hamiltonians  $\{H_0, H_1, \dots, H_{T-1}\}$  and states  $\{|\Psi_0\rangle, |\Psi_1\rangle, \dots, |\Psi_{T-1}\rangle\}$ . Thus the MERA is related to a coarse-graining transformation and naturally leads to a renormalization group flow in both the space of Hamiltonians and states [3], as further discussed in Sects. IV and V. We also notice that a site in  $\mathcal{L}_\tau$  corresponds to a block of  $2^\tau$  sites of  $\mathcal{L}_0$ . Accordingly, lattice  $\mathcal{L}_\tau$  represents the system at length scale  $\lambda_\tau = 2^\tau$  (in distance units given by the separation between nearest sites in  $\mathcal{L}_0$ ).

The key feature of the MERA is that the underlying quantum circuit has a very special causal structure: the causal cone  $\mathcal{C}$  of any outgoing wire has bounded width. For instance, the MERA for the case of a one-dimensional lattice  $\mathcal{L}$ , as shown in Fig. (7), is such that  $\mathcal{C}$  contains at most three sites of each layer  $\mathcal{L}_\tau$ . This property allow us to efficiently compute the reduced density matrix for any outgoing wire of the quantum circuit —equivalently, for each site  $s$  of the original lattice  $\mathcal{L}$  [3]. This is reviewed in Figs. (8)-(10).

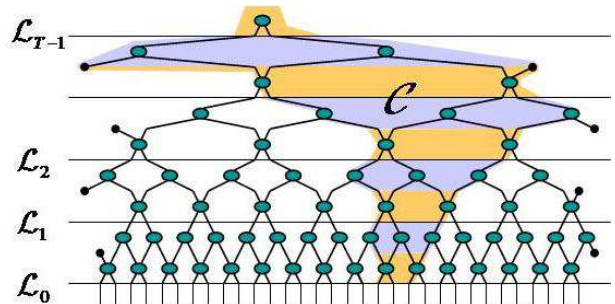


FIG. 7: [Taken from Ref. [3]] A defining property of the MERA is that the causal cone  $\mathcal{C}$  of any small subset of neighboring outgoing wires (equivalently, of sites in  $\mathcal{L}$ ) has finite width. In particular, in a MERA for a one-dimensional lattice the width of the causal cone any outgoing wire is at most 4. Notice that  $\mathcal{C}$  intersects with any effective lattice  $\mathcal{L}_\tau$  through at most three nearest neighboring sites.

#### D. Entanglement renormalization

As explained above, the MERA is closely related to a coarse-graining transformation. The disentanglers  $u$  owe their name to the role they play in such transformation, namely that of reducing the amount of entanglement in the system before the sites of the lattice are coarse-grained. The following example aims to clarify what that means.

Consider a one-dimensional lattice  $\mathcal{L}_0$  in the state  $|\Psi_0\rangle$ ,

$$|\Psi_0\rangle \equiv |\Phi^{[1,2]}\rangle|\Phi^{[3,4]}\rangle \dots |\Phi^{[N-1,N]}\rangle, \quad (7)$$

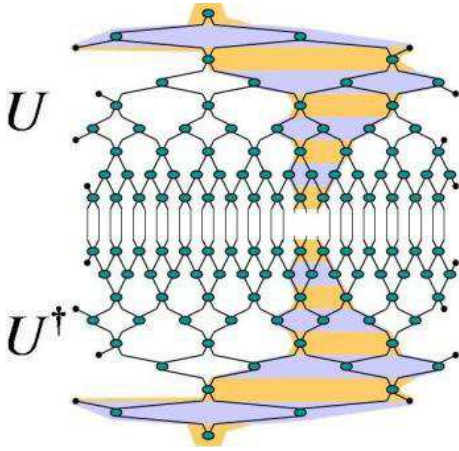


FIG. 8: The computation of the reduced density matrix  $\rho^{[B]} \equiv \text{tr}_{\bar{B}} |\Psi\rangle\langle\Psi|$  for a block  $B$  made of three contiguous sites consists in contracting this tensor network, where the six open wires correspond to the sites of  $\rho^{[B]}$ .

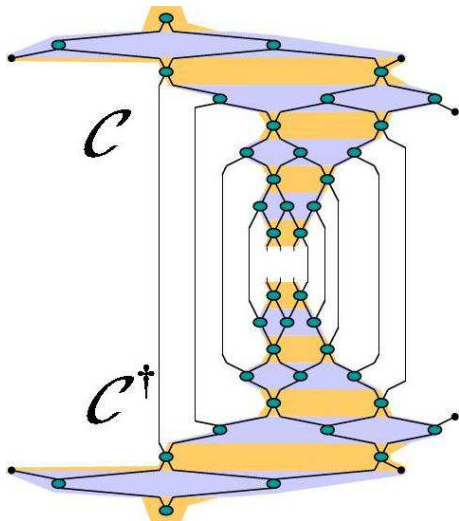


FIG. 9: The tensor network in Fig. (8) is simplified to a tensor network involving only the tensors in the causal cone of  $B$  thanks to the isometric constraints of the tensors in the MERA, see Fig. (5)

made of two-site entangled states  $|\Phi^{[s,s+1]}\rangle$ ,

$$|\Phi^{[s,s+1]}\rangle \equiv \frac{1}{\sqrt{2}}(|0^{[s]}\rangle|0^{[s+1]}\rangle + |1^{[s]}\rangle|1^{[s+1]}\rangle). \quad (8)$$

The reduced density matrix  $\rho^{[2n,2n+1]}$  for a block of two contiguous sites  $[2n, 2n+1] \in \mathcal{L}_0$  has rank 4 and reads

$$\rho^{[2n,2n+1]} = \rho^{[2n]} \otimes \rho^{[2n+1]}, \quad (9)$$

where  $\rho_0^{[s]} = (|0^{[s]}\rangle\langle 0^{[s]}| + |1^{[s]}\rangle\langle 1^{[s]}|)/2$ . Let us create a coarse-grained lattice  $\mathcal{L}_1$  by identifying each site  $s' \in \mathcal{L}_1$  with a block  $[2n, 2n+1] \in \mathcal{L}_0$  by means of an isometry  $w : \mathbb{V}^{[s']} \rightarrow \mathbb{V}^{[2n]} \otimes \mathbb{V}^{[2n+1]}$ , and let  $|\Psi_1\rangle$  be the projection of  $|\Psi_0\rangle$  on  $\mathcal{L}_1$ . Then, if  $|\Psi_1\rangle$  is to retain the properties

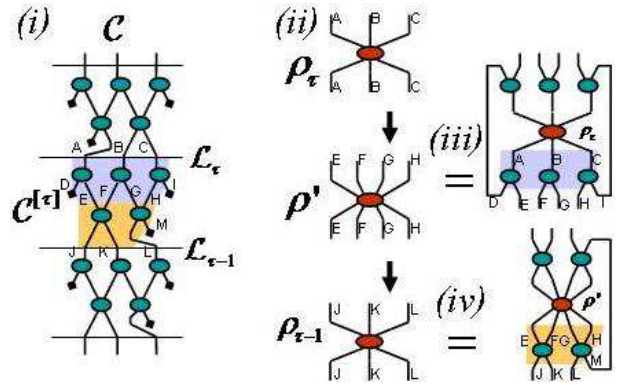


FIG. 10: [Taken from Ref. [3]] The tensor network in Fig. (9) is contracted by descending through the causal cone  $\mathcal{C}$ . (i) Three layers of  $\mathcal{C}$ . (ii) The density matrix  $\rho_{\tau-1}$  is obtained from  $\rho_{\tau}$  and the tensors in  $\mathcal{C}^{[\tau]}$  through matrix multiplications, with a cost  $O(\chi^9)$ .

of  $|\Psi_0\rangle$ , the vector space  $\mathbb{V}^{[s']}$  has to be large enough to support  $\rho^{[2n,2n+1]}$ , which had rank 4. That is, the amount of entanglement between the block  $[2n, 2n+1] \in \mathcal{L}_0$  and its neighboring sites (as measured by the rank of  $\rho^{[2n,2n+1]}$ ) determines that  $\chi_1$  must be at least 4.

The key observation is that we can reduce this entanglement (equivalently, the rank of  $\rho^{[2n,2n+1]}$ ) by using disentanglers, see Fig. (11), resulting in a smaller  $\chi'_1$ . For that we just need to choose the disentangler  $u$  such that it transforms  $|\Phi^{[s,s+1]}\rangle$  into a product state  $|0^{[s]}\rangle|0^{[s+1]}\rangle$ ,

$$|0^{[s]}\rangle|0^{[s+1]}\rangle = u^\dagger |\Phi^{[s,s+1]}\rangle. \quad (10)$$

In summary, the example illustrates how disentanglers can decrease the amount of entanglement in  $|\Psi_0\rangle$ , leading to a more compact coarse-grained description  $|\Psi_1\rangle$ . This fact may not seem of much interest at first sight. One might think that any computational gain based on having a more compact description for  $|\Psi_1\rangle$  will be set off by the costs of finding the disentanglers. This is not the case.

To appreciate the potential gains resulting from entanglement renormalization, we need to consider the growth of the dimension  $\chi_\tau$  of the sites of  $\mathcal{L}_\tau$  with each iteration of the coarse-graining transformation. [For simplicity, in the rest of the manuscript  $\chi_\tau$  has been taken to be a constant  $\chi$  independent of  $\tau$ .] Critical ground states in one spatial dimension and non-critical ground states in two spatial dimensions serve to illustrate this point. A boundary law for entanglement in such systems [10] implies that, *without* disentanglers,  $\chi_\tau$  must grow at least as  $O(\exp(\tau))$  in one spatial dimension and as  $O(\exp(\exp(\tau)))$  in two spatial dimensions. After a few iterations of the coarse-graining transformation  $\chi_\tau$  becomes unaf

The example in Fig. (11) also illustrates another important fact. For the disentanglers to be useful, they need to be chosen carefully. A random choice of  $u$  will fail to disentangle  $|\Phi^{[s,s+1]}\rangle$  in Eq. (8)—as a matter of

fact, a poorly chosen disentangler will result in a final state that is even more entangled than the original one. But optimizing over a set of isometric tensors to compute the disentanglers and isometries is not simple. This will be the focus of the entire next section.

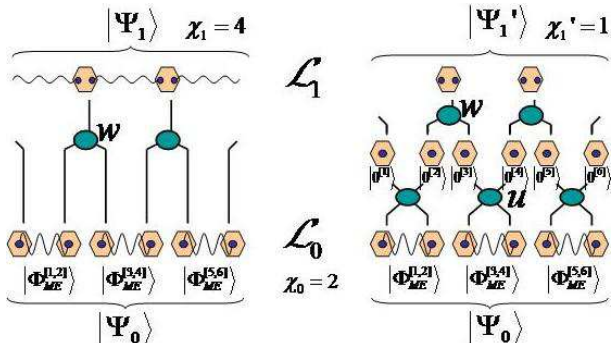


FIG. 11: Coarse-graining scheme without disentanglers (left) and with disentanglers (right). In this example, the dimension  $\chi_1$  of the vector space of the sites in the coarse-grained lattice  $\mathcal{L}_1$  needs to be 4 when no disentanglers are used, if  $|\Psi_1\rangle$  is to retain the properties of  $|\Psi_0\rangle$ . When disentanglers are used,  $\chi_1' = 1$  is enough to support the coarse-grained state  $|\Psi_1'\rangle$ .

### III. LINEAR AND QUADRATIC OPTIMIZATIONS OVER ISOMETRIC TENSORS

In this section we discuss a number of optimizations involving isometric tensors. The strategies that we explore can be applied to the optimization of isometric quantum circuits in general, with disregard of the structure of the circuit [11]. In the present paper, they are used to compute the tensors in the MERA in the algorithms of Sect. IV-??.

The reader primarily interested in the algorithms of Sects. IV-?? may want to skip this section in the first reading of the notes.

#### A. Types of optimizations

Only a subset of the optimizations that we consider can be solved exactly. For the rest, we propose strategies that lead to sub-optimal solutions. Sub-optimal solutions are often good enough in order to build the MERA.

Let us introduce some notation specific to this section. Given an isometric transformation  $U : \mathbb{V}_{in} \rightarrow \mathbb{V}_{out}$ , we denote by  $\mathbf{x} = [U_{11} \dots U_{12} \dots U_{d_{out} d_{in}}]^T$  a column vector with all its entries  $U_{\alpha\beta}$ . If  $U$  is made of smaller gates organized according to a circuit structure  $\mathcal{Q}$ , then we write  $U \in \mathcal{Q}$  and refer to  $U$  as a *constrained* isometric transformation. Instead, if  $U$  is an arbitrary isometric transformation we write  $U \in \mathcal{U}$  and call it *unconstrained*. Obviously, in either case the isometric transformation is always constrained to fulfill  $U^\dagger U = I_{in}$ , so that the label

(un)constrained refers merely to whether the entries of  $U$  are additionally restricted to be compatible with some underlying circuit structure  $\mathcal{Q}$ .

We distinguish between *linear* optimizations and *quadratic* optimizations depending on how the cost function  $f(U)$  depends on  $U$ ; and between *constrained* and *unconstrained* optimizations, depending on whether  $U$  is further constrained by some circuit structure  $\mathcal{Q}$ . More specifically, we address the following four types of optimizations.

- *Unconstrained linear (UL) optimization.*— The cost function  $f(U)$  is linear in the isometric transformation  $U$ ,

$$\max_{U \in \mathcal{U}} |\mathbf{y}^\dagger \cdot \mathbf{x}| = \max_{U \in \mathcal{U}} |\text{tr}(W^\dagger U)|, \quad (11)$$

and there are no additional constraints.

- *Constrained linear (CL) optimization.*— The cost function  $f(U)$  is linear in the isometric transformation  $U$ ,

$$\max_{U \in \mathcal{Q}} |\mathbf{y}^\dagger \cdot \mathbf{x}| = \max_{U \in \mathcal{Q}} |\text{tr}(W^\dagger U)|, \quad (12)$$

and  $U$  is additionally constrained to have a given quantum circuit structure  $\mathcal{Q}$ , see Fig. (12).

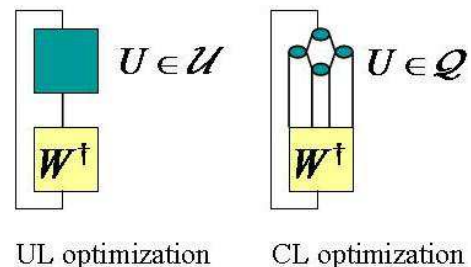


FIG. 12: Diagrammatic representation of the cost function  $f(U) = |\text{tr}(W^\dagger U)|$  for linear optimizations of type UL and CL, see Eqs. (11)-(12).

- *Unconstrained quadratic (UQ) optimization.*— The cost function  $f(U)$  is quadratic in the isometric transformation  $U$ ,

$$\max_{U \in \mathcal{U}} \mathbf{x}^\dagger \cdot K \cdot \mathbf{x} = \max_{U \in \mathcal{U}} \sum_i \text{tr}(U^\dagger M_i U N_i), \quad (13)$$

and there are no additional constraints, see Fig. (13). We only need to consider a hermitian  $K$ ,  $K = K^\dagger$ . We single out the case where  $K$  decomposes into only one  $M$  and  $N$  ( $M = M^\dagger$ ,  $N = N^\dagger$ ), see Fig. (14), that we refer to as *simplified unconstrained quadratic (SUQ) optimization*,

$$\max_{U \in \mathcal{U}} \text{tr}(U^\dagger M U N). \quad (14)$$

- *Constrained quadratic (CQ) optimization.*— The cost function  $f(U)$  is quadratic in the isometric transformation  $U$ ,

$$\max_{U \in \mathcal{Q}} \mathbf{x}^\dagger \cdot K \cdot \mathbf{x} = \max_{U \in \mathcal{Q}} \sum_i \text{tr}(U^\dagger M_i U N_i), \quad (15)$$

and  $U$  is additionally constrained to have a given quantum circuit structure  $\mathcal{Q}$ , see Fig. (13). Again, we only need to consider a hermitian  $K$ ,  $K = K^\dagger$ , and we single out the case where  $K$  decomposes into only one  $M$  and  $N$  ( $M = M^\dagger$ ,  $N = N^\dagger$ ), that we refer to as *simplified constrained quadratic (SCQ) optimization*,

$$\max_{U \in \mathcal{Q}} \text{tr}(U^\dagger M U N). \quad (16)$$

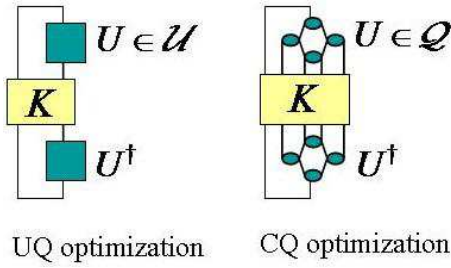


FIG. 13: Diagrammatic representation of the cost function  $f(U)$  for quadratic optimizations UL and CL, see Eqs. (13) and (15).

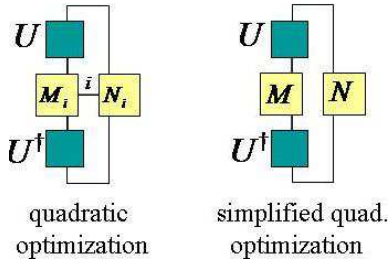


FIG. 14: In a simplified quadratic optimization there is only one pair of matrices  $M$  and  $N$ ,  $f(U) = U^\dagger M U N$ .

Notice that any linear maximization over the isometric transformation  $U$ , namely types UL and CL above, is equivalent to a minimization of the form

$$\min_{U \in \mathcal{Q}} \|W - U\|^2, \quad (17)$$

where  $\|A\|$  denotes the Frobenius norm,  $\|A\|^2 \equiv \text{tr}(A^\dagger A)$ . Indeed, for an arbitrary isometric transformation  $U$  we have

$$\|W - U\|^2 = \text{tr}((W - U)^\dagger (W - U)) \quad (18)$$

$$= \text{tr}(W^\dagger W) + \text{tr}(U^\dagger U) - (\text{tr}(W^\dagger U) + c.c.) \quad (19)$$

$$= \text{const.} - (\text{tr}(W^\dagger U) + \text{tr}(W U^\dagger)), \quad (20)$$

and therefore

$$\min_U \|W - U\|^2 = \text{const.} - 2 \max_U |\text{tr}(W^\dagger U)|, \quad (21)$$

where we have used that for any isometric transformation  $U_0$ , there always exist a phase  $e^{i\phi}$  such that  $\text{tr}(W^\dagger U)$  is real for  $U = e^{i\phi} U_0$ , and thus  $2|\text{tr}(W^\dagger U)| = \text{tr}(W^\dagger U) + \text{tr}(W U^\dagger)$ . It follows that the methods we discuss for UL and CL optimizations can all be reformulated as least square methods for isometric tensors.

## B. Reductions

From all the types described above, only some of the unconstrained optimizations, namely types UL and SUQ, turn out to have analytical solutions. For the rest of optimizations, we propose several strategies.

The remaining unconstrained optimizations, that is, optimizations of type UQ that are not of type SUQ, are addressed either through a steepest descent approach or by linearizing the cost function. Then, having a strategy for each type of unconstrained optimization, we can move to address the constrained types CL and CQ. This is often done by replacing a constrained optimization CL or CQ with a series of alternating unconstrained optimizations UL, SUQ or UQ. Fig. (15) summarizes a number of possible reductions between types of optimizations.

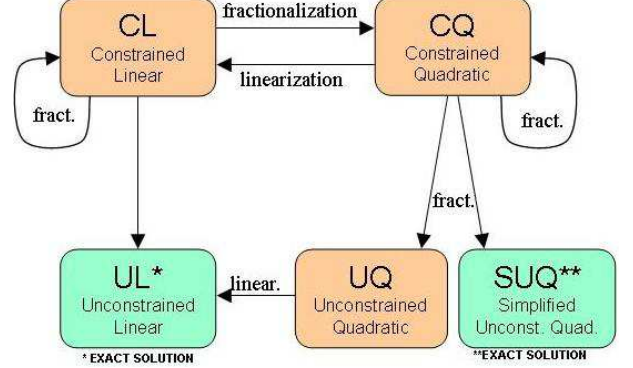


FIG. 15: Diagram representing several reductions between different types of optimizations. Unconstrained types UL and SUQ can be *solved exactly*. By *linearization* of the cost function, quadratic types CQ and UQ are replaced with linear types CL and UL. By *fractionalization*, constrained types CL and CQ are replaced with an alternating series of simpler optimizations.

The rest of this section is devoted to addressing each type of optimization. We start by reviewing the exact solution of types UL and SUQ. Then we discuss in some detail type UQ. Finally we explain how types CL and CQ can be reduced to unconstrained optimizations of type UL and UQ.

We emphasize that except for types UL and SUQ, that can be solved exactly, none of the optimization strategies

that we discuss is guaranteed to converge to the optimal solution. Some strategies are not even guaranteed to converge at all. Or, when they do converge, we cannot know whether the solution is optimal. However, the merit of these strategies relies in that they have proved to be valuable in the context of entanglement renormalization and the MERA. There, a suboptimal  $U$  that leads to a comparatively large value of the cost function  $f(U)$  might already be good enough to ensure the success of the simulation algorithm. We also stress that in this manuscript we simply describe these optimization strategies but make no attempt to justify why they should be expected to work.

### C. UL optimization

We would like to maximize the cost function

$$f(U) \equiv |\text{tr}(W^\dagger U)| \quad (22)$$

over all isometric transformations  $U \in \mathcal{U}$ . Let  $W = XSY^\dagger$  be the singular value decomposition [12] of matrix  $W$  and let  $r$  be its rank. Here  $X$  and  $Y$  are isometric matrices and  $S$  is a diagonal matrix with the  $r$  (decreasingly ordered) non-zero singular values  $s_1 \geq s_2 \geq \dots \geq s_r > 0$  of  $W$ . Then  $f(U)$  achieves its maximum for  $U = XY^\dagger$ , and we obtain

$$\max_{U \in \mathcal{U}} |\text{tr}(W^\dagger U)| = \text{tr}(YSX^\dagger XY^\dagger) = \text{tr}(S) = \sum_{k=1}^r s_k. \quad (23)$$

If  $U$  is additionally restricted to have rank  $r'$ ,  $r' < r$ , then the optimal choice reads  $U = XQ_{r'}Y^\dagger$ , where  $Q_{r'}$  is a diagonal matrix with ones on the first  $r'$  diagonal entries and zeros elsewhere, and the optimal value of the trace is given by the sum  $\sum_{k=1}^{r'} s_k$  of the  $r'$  largest singular values of  $W$ .

As examples of UL optimizations, consider Figs. (29), (30), (34), (??) and (??), which are concerned with the computation of either a disentangler  $u$  or an isometry  $w$  for the MERA.

### D. SUQ optimization

Here we would like to maximize the cost function

$$f(U) \equiv \text{tr}(U^\dagger MUN), \quad (24)$$

where  $M^\dagger = M$  and  $N^\dagger = N$ , over all isometric transformations  $U \in \mathcal{U}$ . Let  $M = XDX^\dagger$  and  $N = YEY^\dagger$  be the eigenvalue decompositions [12] of the  $r \times r$  matrix  $M$  and  $s \times s$  matrix  $N$  in Eq. (14). Here  $X$  and  $Y$  are unitary matrices and  $D$  and  $E$  are diagonal matrices with the diagonal entries given by the (decreasingly ordered) eigenvalues  $m_1 \geq m_2 \dots \geq m_r$  and  $n_1 \geq n_2 \dots \geq n_s$  of  $M$  and  $N$ . For simplicity, we assume that none of the

eigenvalues  $n_k$  of  $N$  is negative (a slightly more complicated exact solution also exists otherwise). Then the cost function  $f(U) = \text{tr}(U^\dagger MUN)$  achieves its maximum for  $U = X^\dagger Y$ , which leads to

$$\max_{U \in \mathcal{U}} \text{tr}(U^\dagger MUN) = \sum_{k=1}^{\min(r,s)} m_k n_k. \quad (25)$$

If  $U$  is constrained to have rank  $r'$  smaller than  $r$  and  $s$ , then the optimal  $U$  reads  $U = X^\dagger Q_{r'} Y$ , where  $Q_{r'}$  is a diagonal matrix with ones on the first  $r'$  diagonal entries and zeros elsewhere, and the optimal value of the trace is given by the sum  $\sum_{k=1}^{r'} m_k n_k$ .

We notice that when  $N$  is the identity and  $r' \leq \min(r, s)$ , the SUQ optimization finds a projector  $P \equiv UU^\dagger$  onto the subspace containing the  $r'$  largest eigenvectors of  $M$ ,

$$\text{tr}(P^\dagger MP) = \sum_{k=1}^{r'} m_k. \quad (26)$$

As examples of SUQ optimizations, consider Figs. (24) and (32), which are concerned with the computation of an isometry  $w$  for the MERA.

### E. UQ optimization

UQ optimizations are the simplest type that we can not solve exactly. Given its importance in the context of computing disentanglers, we describe three different strategies to address them. Recall that our goal is to maximize the cost function

$$f(U) \equiv \sum_i \text{tr}(U^\dagger M_i U N_i) \quad (27)$$

over all isometric transformations  $U \in \mathcal{U}$ .

*Steepest descent.*— A simple approach to a UQ optimization is to use steepest descent (or gradient) methods in the space of isometric transformations  $U \in \mathcal{U}$ . Given an initial  $U_0$ , a family of isometric transformations  $U_0(t) \equiv U_0 \exp(-i\tilde{H}t)$  [with suitable arrangements if  $U$  is not a square matrix] is obtained analytically by determining the direction  $\tilde{H}$ ,  $\|\tilde{H}\| = 1$ , of maximal change in  $t$  of the cost function  $f(U)$ , namely the solution of

$$\frac{df}{dt}\Big|_{t=0} = \text{tr}[\tilde{H} \sum_i (U_0^\dagger M_i U_0 N_i - N_i U_0^\dagger M_i U_0)] = 0. \quad (28)$$

After determining  $\tilde{H}$ , a one-dimensional maximization over the family  $U_0(t)$ , with  $t \in [0, T]$  for some  $T$ , leads to a gate  $U_1$  better than  $U_0$ , that is  $f(U_1) \geq f(U_0)$ . This concludes the basic step of the strategy. Now we can use  $U_1$  to define a new family  $U_1(t) \equiv U_1 \exp(-i\tilde{H}t)$ , and so on. Upon iteration, we obtain a sequence of gates  $\{U_0, U_1, U_2, \dots\}$ . We keep iterating the basic step until the cost function  $f(U)$  has converged.

While steepest descent methods work reasonably well, we find that other strategies, based on linearizing the cost function  $f(U)$ , are generally much faster and often provide a better solution.

*Linearization I.*— A second method to address a UQ optimization consists in regarding Eq. (13) as a linear optimization for  $U$  while keeping  $U^\dagger$  fixed. Let  $U_0$  be an initial isometric transformation. Then, starting with  $k = 1$  and for increasing values  $k = 1, 2, \dots$ , we obtain  $U_k$  from  $U_{k-1}$  by optimizing

$$\max_{U_k \in \mathcal{U}} \sum_i \text{tr}(U_{k-1}^\dagger M_i U_k N_i) = \max_{U_k \in \mathcal{U}} \text{tr}(W_{k-1} U_k), \quad (29)$$

where  $W_{k-1} \equiv \sum_i N_i U_{k-1}^\dagger M_i$ . This is an UL optimization and thus we can solve it exactly. The process is iterated until the sequence of gates  $\{U_0, U_1, U_2, \dots\}$  convergence. Notice that the cost function  $f(U_p)$  is not necessarily improved at each step, nor is convergence guaranteed. However, we find that this method typically converges, it does it fast and produces a good isometric transformation  $U$ .

*Linearization II.*— Our final method to address a UQ optimization consists in regarding  $U$  and  $U^\dagger$  as independent isometric transformations  $U$  and  $V^\dagger$ , while requiring that  $V = U$  through a "soft" constraint. We use an alternating UL optimization to address

$$\max_{U, V \in \mathcal{U}} \sum_i \text{tr}(V^\dagger M_i U N_i) + \lambda \text{tr}(V^\dagger U), \quad (30)$$

where  $\lambda > 0$  is a constant chosen ad hoc, typically of order 1. In this case the modified cost function  $f(U, V) \equiv \sum_i \text{tr}(V^\dagger M_i U N_i) + \lambda \text{tr}(V^\dagger U)$ , see Fig. (16) is guaranteed to increase step by step (if  $\lambda$  is fixed) and thus to eventually converge to some maximum for some pair  $(U_f, V_f)$ . In practice, at the end of the alternating sequence of UL optimizations we seem to typically obtain  $V_f = U_f$ , as needed; whenever this is not the case and  $V_f \neq U_f$ , the UQ optimization is repeated but with a larger value for  $\lambda$ , which can also be increased during the iterations. This method consistently provides the best final isometric transformation  $U$  and it is nearly as fast as the previous one.

As examples of UQ optimizations, consider Figs. (23) and (31), which are concerned with the computation of a disentangler  $u$  for the MERA.

## F. CL optimizations

Here our aim is to maximize the cost function

$$f(U) \equiv |\text{tr}(W^\dagger U)| \quad (31)$$

over the set of isometric transformations  $U \in \mathcal{Q}$  constrained by some circuit structure  $\mathcal{Q}$ . Recall that  $U$  depends linearly on each of the isometric tensors  $u_i$  that form the isometric quantum circuit  $\mathcal{Q}$ ,  $U = q(u_1, u_2, \dots, u_p)$ .

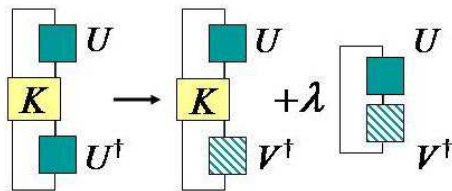


FIG. 16: Example of linearization of a quadratic optimization. A UQ optimization can be addressed by considering  $U$  and  $V^\dagger \equiv U^\dagger$  as independent isometric transformations, only linked through the  $\lambda$  term in the cost function. Then an alternating LU optimization is applied during which  $\lambda$  is increased in order to eventually ensure that  $U = V$ . The resulting  $U$  is not guaranteed to be optimal.

A natural strategy to address a CL optimization over the constrained  $U$  is to fractionalize it into a series of alternating UL optimizations over each of the unconstrained isometric tensors  $u_i$ . For instance, given a set of initial tensors  $\{u_1, u_2, u_3 \dots u_q\}$ , first tensor  $u_1$  is improved to  $u'_1$ , while keeping the rest of tensors fixed, through a UL optimization. Then  $u_2$  is UL optimized for fixed  $\{u'_1, u_3, \dots, u_p\}$ . More generally, each  $u_i$  is sequentially UL optimized while keeping the rest of tensors fixed to their most recent updated form.

Notice that the cost function  $f_i(u_i) \equiv \text{tr}(W_i^\dagger u_i)$  for the individual LU optimization of the isometric tensor  $u_i$  is equal to the cost function  $f(U) \equiv \text{tr}(W^\dagger U)$  for the global CL optimization,

$$f(U) \equiv \text{tr}(W^\dagger U) = \text{tr}(W^\dagger q(\{\dots, u_i, \dots\})) \quad (32)$$

$$= \text{tr}(W_i^\dagger u_i) \equiv f_i(u_i). \quad (33)$$

Therefore the global cost function  $f(U)$  can only increase every time a tensor  $u_i$  is updated. The series of alternating UL optimizations over isometric tensors  $u_i$  can be repeated until the cost function  $f(U)$  converges.

There are multiple ways to build a sequence of UL optimizations. For instance, one can build a list with all the individual  $u_i$  and proceed in that order. Or one could choose the individual gate  $u_i$  to be optimized at random. The choice of a particular sequence often affects the computational cost involved in computing the tensors  $W_i$ , which is obtained by contracting some tensor network, and can be tailored to minimize this cost. In particular, in the case when  $U$  is a MERA, we will organize such optimizations in layers in order to exploit its peculiar causal structure.

We note that this approach to constrained optimizations is similar to the alternating least squares method that Verstraete, Cirac and collaborators have extensively used to optimize (non-isometric) tensor networks in the context of MPS [13] and PEPS algorithms [9]. In the present case, a number of additional arrangements are necessary in order to deal with isometric tensors  $u_i$  (e.g., because the UQ type can no longer be solved exactly, in contrast with its non-isometric version).

As examples of CL optimizations, consider Figs. (27),

(??), (??) and (??), which involve the MERA. In all these cases, we address the optimization by fractionalizing it into a series of alternating UL optimizations.

### G. CQ optimizations

A CQ optimization can be similarly addressed by fractionalizing it into a series of alternating UQ optimizations, and this is our standard approach.

Alternatively, one attempt one of several linearization strategies. Two possibilities are given by variants of the linearized approaches discussed for UQ optimizations. Another possibility, specific for the SCQ type, is discussed in Fig. (17).

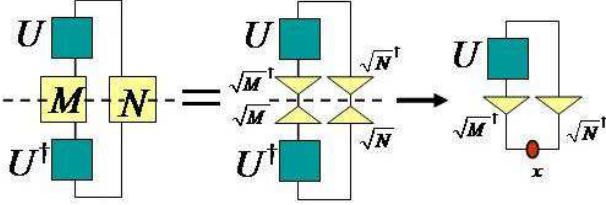


FIG. 17: Example of linearization of a simplified quadratic optimization. This is of interest for SCQ optimizations, but for simplicity the figure represents the cost function of an (exactly solvable) SUQ. The cost function  $f(U) = \text{tr}(U^\dagger M U N)$  is expressed as  $\text{tr}(E^\dagger E)$ , where  $E = \sqrt{N}^\dagger U \sqrt{M}$ . We then optimize the cost function  $g(U) = \text{tr}(x E)$  through alternating UL optimizations over  $U$  and the auxiliary isometry  $x$ . As with most strategies discussed in this section, the resulting  $U$  is not guaranteed to be optimal, but has proved useful in the context of optimizing the MERA.

Examples of CQ optimizations involving the MERA are given by Figs. (19), (22) and (26).

## IV. ENTANGLEMENT RENORMALIZATION FOR MANY-BODY HAMILTONIANS

In this section we describe an algorithm to build a MERA for the low energy subspace of a local Hamiltonian  $H$ . For simplicity, we consider a system in  $D = 1$  spatial dimensions only. A generalization of this algorithm to deal with systems in  $D > 1$  dimensions, using the  $D$ -dimensional MERA, is conceptually straightforward.

### A. A real space RG transformation for Hamiltonians

We consider a many-body system characterized by a lattice  $\mathcal{L}$  in  $D = 1$  spatial dimensions made of  $N$  sites ( $N = 2^T$  for some integer  $T$ ) and a local Hamiltonian  $H : \mathbb{V}^{\otimes N} \rightarrow \mathbb{V}^{\otimes N}$  that decomposes as

$$H = \sum_s h^{[s]}, \quad (34)$$

where the term  $h^{[s]}$  acts on a block of three consecutive sites  $[s, s+1, s+2] \in \mathcal{L}$ . Notice that this includes the case of a Hamiltonian made of two-body terms acting on contiguous sites [14].

As explained in section II, the MERA is naturally linked to a coarse-graining transformation that creates a sequence of effective Hamiltonians  $\{H_0, H_1, \dots, H_{T-1}\}$ , for the increasingly coarse-grained lattices effective lattices  $\{\mathcal{L}_0, \mathcal{L}_1, \dots, \mathcal{L}_{T-1}\}$ . Here  $H_0 \equiv H$ ,  $\mathcal{L}_0 \equiv \mathcal{L}$  and lattice  $\mathcal{L}_\tau$  describes the system at a length scale  $\lambda_\tau = 2^\tau$ . In addition, thanks to the causal structure of the MERA, Hamiltonian  $H_\tau$  is local and made of three-site terms, just as the original  $H$ . Thus, the coarse-graining transformation can be understood as a real space renormalization group (RG) transformation and the sequence  $\{H_0, H_1, H_2, \dots\}$  defines a RG flow in the space of local Hamiltonians. This RG flow is irreversible in that  $H_\tau$  only retains the low energy properties of  $H_{\tau-1}$ , and information about high energy properties are lost. In the limit of an infinite lattice  $\mathcal{L}$ , and when the initial Hamiltonian  $H$  corresponds to a quantum critical system, this RG flow is numerically seen to converge to a fixed point [4].

### B. MERA for the low energy subspace of a local Hamiltonian.

We use a rank  $r$  MERA ( $r > 1$ ), denoted  $\mathcal{M}_r$ , to encode (an approximation to) the low energy subspace of Hamiltonian  $H$ , that is the subspace containing the  $r$  eigenvectors of  $H$  with smallest eigenvalues. In this case the top tensor of the MERA has an open wire to account for  $r$  dimensions. If  $U \in \mathcal{M}_r$  is the isometric transformation corresponding to the MERA, so that  $P(U) \equiv U U^\dagger$  is a projector onto a subspace of dimension  $r$ , our goal is to find  $U$  such that it minimizes the expectation value for the energy

$$\min_{U \in \mathcal{M}_r} \text{tr}(U^\dagger H U) = \min_{U \in \mathcal{M}_r} \text{tr}(P(U) H P(U)^\dagger). \quad (35)$$

This is an optimization of type SCQ and corresponds to Eq. (16) with the substitutions  $M = -H$  and  $N = I_r$  ( $I_r$  is the identity operator in an  $r$ -dimensional space).

The optimization of Eq. (35) can be addressed in multiple ways. One option is to replace it with a sequence of alternating UQ optimizations over all disentanglers  $u$  and isometries  $w$  of the MERA, and to repeat the sequence until the cost function  $f(U) = \text{tr}(U^\dagger H U)$  has converged. We find that a particularly convenient way to organize an alternating strategy consists in optimizing the MERA layer by layer. In this manner the causal structure of the MERA can be best exploited to minimize computational costs, the results are very robust, and the scheme can be modified to address systems with translational invariance with a cost logarithmic in the system size.

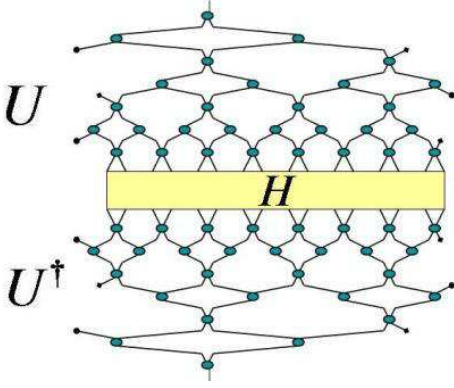


FIG. 18: Tensor network representation of  $H_T \equiv U^\dagger H U$ , where  $U \in \mathcal{M}_r$  is an isometric transformation that encodes the subspace of dimension  $r$  spanned by the eigenvectors of  $H$  with minimal energy. The algorithm can be used e.g. to study topologically degenerate ground states.

### C. Layered optimization

Thus we replace the SCQ optimization (35) over  $U \in \mathcal{M}_r$  with a sequence of alternating SCQ optimizations for the isometric transformations  $U^{[\tau]}$  corresponding to different layers of the MERA. Later we will explain how to address these SCQ optimizations by further decomposing them into simpler optimizations. The algorithm starts with an *initialization stage*, during which each  $U^{[\tau]}$  is created. This is followed by a *convergence stage* that further optimizes the  $U^{[\tau]}$  of the MERA by sequentially and repeatedly sweeping over all length scales in the system.

*Initialization stage.*— We initialize the MERA by performing a series of SCQ optimizations of the form

$$\min_{U^{[\tau]} \in \mathcal{M}^{[\tau]}} \text{tr}(U^{[\tau]\dagger} H_{\tau-1} U^{[\tau]}), \quad (36)$$

where  $H_{\tau-1}$  is an effective Hamiltonian and  $U^{[\tau]} \in \mathcal{M}^{[\tau]}$  is restricted by the circuit structure  $\mathcal{M}^{[\tau]}$ , made of one row of disentglers and one row of isometries, see Fig. (19).

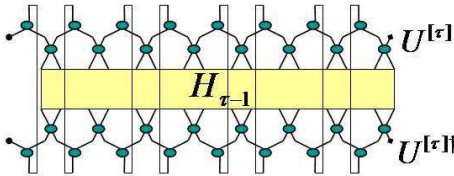


FIG. 19: Diagrammatic representation of the cost function in the optimization of  $U^{[\tau]}$  in Eq. (36). This cost function breaks into local pieces, see Fig. (22).

The initialization stage works by addressing the MERA layer by layer, from short length scales to large length scales. Starting with  $\tau = 1$ , we repeat the following two steps for increasing values of  $\tau$ ,  $1 \leq \tau \leq T - 1$ .

A1. Given Hamiltonian  $H_{\tau-1}$  for lattice  $\mathcal{L}_{\tau-1}$ , obtain the isometric transformation  $U^{[\tau]}$  according to optimization (36).

A2. Given Hamiltonian  $H_{\tau-1}$  and  $U^{[\tau]}$ , construct a Hamiltonian  $H_\tau = U^{[\tau]\dagger} H_{\tau-1} U^{[\tau]}$  for  $\mathcal{L}_\tau$ , see Fig. (20).

Iteration over  $\tau$  produces a sequence of increasingly coarse-grained effective Hamiltonians and isometric transformations,

$$H_0 \rightarrow U^{[1]} \rightarrow H_1 \rightarrow U^{[2]} \rightarrow H_2 \rightarrow \dots \rightarrow H_{T-1} \rightarrow U^{[T]}. \quad (37)$$

The MERA is thus initialized to  $U \in \mathcal{M}$  as  $U = U^{[1]} U^{[2]} \dots U^{[T]}$ , where the top isometric transformation  $U^{[T]}$  has been obtained by direct diagonalization of  $H_{T-1}$  (notice that  $U^{[T]}$  projects onto a subspace spanned by the  $r$  eigenvectors of  $H_{T-1}$  with smallest eigenvalues).

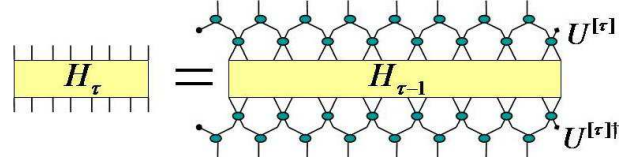


FIG. 20: Effective Hamiltonian  $H_\tau = U^{[\tau]\dagger} H_{\tau-1} U^{[\tau]}$ , see also Fig. (21).

*Convergence stage.*— The MERA can now be further improved. For each value of  $\tau$ , we consider the SCQ optimization

$$\min_{U^{[\tau]} \in \mathcal{M}^{[\tau]}} \text{tr}(U^{[\tau]\dagger} H_{\tau-1} U^{[\tau]} P_\tau), \quad (38)$$

where  $P_\tau$  is a projector defined as

$$P_\tau \equiv \left( U^{[\tau+1]} \dots U^{[T]} \right) \left( U^{[\tau+1]} \dots U^{[T]} \right)^\dagger, \quad (39)$$

so that  $U^{[\tau]}$  is now optimized taking into account not only all the lower layers of the MERA  $\{U^{[1]}, \dots, U^{[\tau-1]}\}$ , which determine  $H_{\tau-1}$ , but also all the upper layers of the MERA  $\{U^{[\tau+1]}, \dots, U^{[T]}\}$ .

This part of the algorithm works by sweeping over all layers of the MERA, starting with the top layer ( $\tau = T$ ), then descending layer by layer to the lowest one  $\tau = 1$ , then ascending back to the top. The sweeping is repeated until the cost function converges. During the descent, the two following steps are performed for each value of  $\tau$ :

B1. Given  $H_{\tau-1}$  and  $P_\tau$ , update  $U^{[\tau]}$  according to optimization (38).

B2. Given  $P_\tau$  and the updated  $U^{[\tau]}$ , build  $P_{\tau-1}$  as  $P_{\tau-1} = U^{[\tau]} P_\tau U^{[\tau]\dagger}$ .

During the ascent, the two steps to be performed for each value of  $\tau$  are the following:

- C1. Given  $H_{\tau-1}$  and  $P_\tau$ , update  $U^{[\tau]}$  according to optimization (38).
- C2. Given  $H_{\tau-1}$  and the updated  $U^{[\tau]}$ , update  $H_\tau = U^{[\tau]\dagger} H_{\tau-1} U^{[\tau]}$ .

[We will see that in practice  $P_\tau$  is not needed. We use instead a collection of simpler, related operators  $P_\tau^{[s]}$ ].

We find that whereas the convergence stage improves the MERA and effective Hamiltonians, the initialization stage alone often already produces a good result. The initialization stage turns out to be very insensitive to the global structure of the system - it hardly sees its size or boundary conditions. This can be exploited in the context of calculations involving infinite systems or to study finite size scaling, where some of the results of optimizations for a given system size can be reused for other system sizes.

#### D. Optimization of one layer

Next we explain how to perform the optimizations (36) and (38) for one layer of the MERA during the initialization and convergence stages of the algorithm. We exploit the fact that the Hamiltonian  $H_\tau$  decomposes as the sum of local terms  $h_\tau^{[s]}$  to break the cost functions also into a sum of terms, see Fig. (22). This facilitates enormously the optimization of individual tensors (that is disentanglers and isometries) within  $U^{[\tau]}$ .

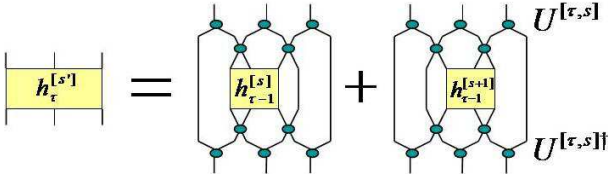


FIG. 21: Hamiltonian term  $h_\tau^{[s']} = U^{[\tau,s]\dagger} (h_{\tau-1}^{[s]} + h_{\tau-1}^{[s+1]}) U^{[\tau,s]}$ , where  $s' \in \mathcal{L}_\tau$  and  $s \in \mathcal{L}_{\tau-1}$ . In this way we obtain the local Hamiltonian  $H_\tau = U^{[\tau]\dagger} H_{\tau-1} U^{[\tau]}$  of Fig. (20) term by term.

We consider first the optimization of  $U^{[\tau]}$  during the initialization stage, Eq. (36). This is performed by repeated horizontal sweeps over the entire layer. For instance, a possible elementary round (to be repeated until convergence of the cost function) consists of the following steps:

- D1. Starting with  $s = 1$  and progressing for all possible odd values of  $s$ ,  $s = 1, 3, 5, \dots$ , update the disentangler  $u^{[\tau,s]}$  by means of a UQ optimization.
- D2. Starting with  $s = 1$  and progressing for all possible odd values of  $s$ ,  $s = 1, 3, 5, \dots$ , update the isometry  $w^{[\tau,s+1]}$  by means of a SUQ optimization.

Importantly, the above optimizations can be done by considering only a small subset of gates in  $U^{[\tau]}$ . This is

due to the fact that the cost function of the optimization (36) decomposes as

$$\begin{aligned} \text{tr}(U^{[\tau]\dagger} H_{\tau-1} U^{[\tau]}) &= \sum_s \text{tr}(U^{[\tau]\dagger} h_{\tau-1}^{[s]} U^{[\tau]}) \quad (40) \\ &= \sum_{\text{odd } s} \text{tr}(U^{[\tau,s]\dagger} (h_{\tau-1}^{[s]} + h_{\tau-1}^{[s+1]}) U^{[\tau,s]}), \quad (41) \end{aligned}$$

where  $U^{[\tau,s]} \equiv (w^{[\tau,s-1]} w^{[\tau,s+1]} w^{[\tau,s+3]}) (u^{[\tau,s]} u^{[\tau,s+2]})$  is an isometry that acts on a block of six consecutive sites  $[s-1, s, \dots, s+4]$  of  $\mathcal{L}_{\tau-1}$  and is made of two disentanglers  $\{u^{[\tau,s]}, u^{[\tau,s+2]}\}$  acting on blocks  $[s, s+1]$  and  $[s+2, s+3]$  respectively, and three isometries  $\{w^{[\tau,s-1]}, w^{[\tau,s+1]}, w^{[\tau,s+3]}\}$  acting on blocks  $[s-1, s]$ ,  $[s+1, s+2]$  and  $[s+3, s+4]$  respectively, see Fig. (21).

It is easy to see that the disentangler  $u^{[\tau,s]}$  is only present in  $U^{[\tau,s-2]}$  and  $U^{\tau,s}$ . Therefore only 4 Hamiltonian terms and 6 other gates enter the cost function for the optimization of  $u^{[\tau,s]}$ , see Fig. (23). Similarly, the isometry  $w^{[\tau,s+1]}$  only appears in  $U^{[\tau,s-2]}$ ,  $U^{\tau,s}$  and  $U^{\tau,s+2}$ , so that only 6 Hamiltonian terms and 8 other gates are involved in the cost function for its optimization, see Fig. (24).

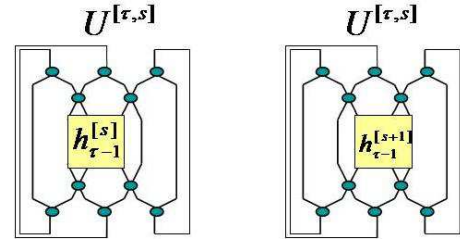


FIG. 22: The cost function  $\text{tr}(U^{[\tau]\dagger} H_{\tau-1} U^{[\tau]})$  in Eq. (36) breaks into pieces, one for each term  $h_{\tau-1}^{[s]}$  of the Hamiltonian  $H_{\tau-1}$ . Here we represent the two terms involving the isometric transformation  $U^{[\tau,s]}$  of Eq. (43).

The optimization of  $U^{[\tau]}$  during the convergence stage follows the same pattern as during the initialization stage, with a sequence of elementary rounds. However, now the figure of merits breaks into pieces according to

$$\begin{aligned} \text{tr}(U^{[\tau]\dagger} H_{\tau-1} U^{[\tau]} P_\tau) &= \sum_r \text{tr}(U^{[\tau]\dagger} h_{\tau-1}^{[s]} U^{[\tau]} P_\tau) \quad (42) \\ &= \sum_{\text{odd } r} \text{tr}(U^{[\tau,s]\dagger} (h_{\tau-1}^{[s]} + h_{\tau-1}^{[s+1]}) U^{[\tau,s]} P_\tau^{[s]}), \quad (43) \end{aligned}$$

where  $P_\tau^{[s]}$  is the restriction of  $P_\tau$  to the relevant sites. Therefore  $P_\tau$  is never required in practice, and is replaced with a full collection of  $P_\tau^{[s]}$  ( $r = 1, 3, 5, \dots$ ). Operator  $P_{\tau-1}^{[s]}$  is obtained from an analogous operator  $P_\tau^{[s']}$  in an identical way as the reduced density matrix  $\rho_{\tau-1}$  is computed from  $\rho_\tau$  in Fig. (10).

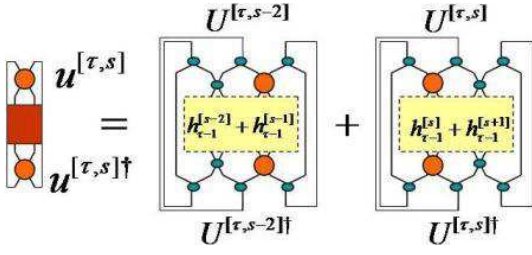


FIG. 23: Cost function  $\mathbf{x}^\dagger K \mathbf{x} = \sum_i \text{tr}(u^{[\tau,s]\dagger} M_i u^{[\tau,s]} N_i)$  in Eq. (13) for the optimization of disentangler  $u^{[\tau,s]}$ . This UQ optimization can be addressed using the strategies described in Sect. III E, with cost  $O(\chi^9)$ , by exploiting the tensor network structure of  $K$ .

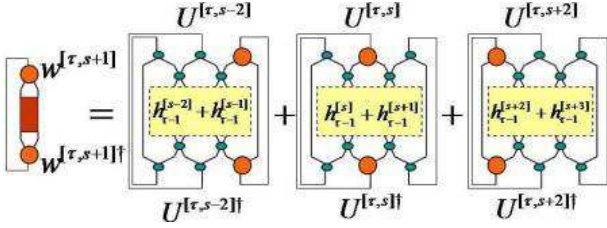


FIG. 24: Cost function  $\mathbf{x}^\dagger K \mathbf{x} = \text{tr}(w^{[\tau,s+1]\dagger} M w^{[\tau,s+1]})$  in Eq. (14) for the optimization of isometry  $w^{[\tau,s+1]}$ . This SUQ optimization can be addressed exactly, see Sect. III D, after building  $M$  with  $O(\chi^9)$  operations.

### E. Computational cost

The optimization of the isometric transformation  $U^{[\tau]}$  requires a number of operations proportional to the number of sites in  $\mathcal{L}_\tau$ . These operations can be reduced to tensor manipulations (matrix multiplications and singular value decompositions), all of which can be accomplished with a cost that scales at most as  $\chi^9$ . Thus, the cost of sweeping over all length scales once is  $O(N\chi^9)$ —notice that the total number of sites in all the effective lattices (as well as the total number of disentanglers and isometries in the MERA) is just  $O(N)$ .

The layered optimization that we have described naturally exploits the fact that the cost function decomposes into pieces; and, by addressing different length scales one by one, it leads to a robust and homogeneous update of the MERA that reuses many partial calculations (as e.g. exemplified by  $P_\tau^{[s]}$ ). Perhaps the most notorious computational advantage is obtained when the Hamiltonian  $H$  is invariant under translations (in a system with periodic boundary conditions). There we can enforce the MERA (and thus the effective Hamiltonians) to be also invariant under translations, e.g. by requiring that all the disentanglers and isometries in a layer be the same. In that case, only a constant number of tensors need to be optimized in each layer, with cost  $O(\chi^9)$ , so that a whole sweep over length scales is accomplished with just  $O(\log(N)\chi^9)$  operations. Finally, an infinite system (open or periodic boundary conditions) can also

be similarly considered to any given length scale  $\lambda_\tau = 2^\tau$ , with a cost  $O(\tau\chi^9)$ .

## V. ENTANGLEMENT RENORMALIZATION FOR MANY-BODY STATES

In this section we describe an algorithm to re-express as a MERA an existing representation for a state  $|\Psi\rangle$ . For simplicity we consider mainly a system in  $D = 1$  spatial dimensions. A generalization of this algorithm to deal with systems in  $D > 1$  dimensions, using the  $D$ -dimensional MERA, is conceptually straightforward, and partially discussed.

We start by discussing an RG flow in the space of states, which sets the stage for the discussion of the algorithm.

### A. A real space RG transformation for states

We consider a many-body system characterized by a lattice  $\mathcal{L}$  in  $D = 1$  spatial dimensions made of  $N$  sites ( $N = 2^T$  for some integer  $T$ ) and a state  $|\Psi\rangle \in \mathbb{V}^{\otimes N}$  that can be written as a MERA.

As in previous sections, we consider the sequence of increasingly coarse-grained lattices  $\{\mathcal{L}_0, \mathcal{L}_1, \dots, \mathcal{L}_{T-1}\}$  induced by the MERA, where  $\mathcal{L}_0 \equiv \mathcal{L}$  and lattice  $\mathcal{L}_\tau$  is associated with length scale  $\lambda_\tau = 2^\tau$ . We also consider the corresponding sequence of states  $\{|\Psi_0\rangle, |\Psi_1\rangle, \dots, |\Psi_{T-1}\rangle\}$ , where  $|\Psi_0\rangle \equiv |\Psi\rangle$ . We notice that all the states of this sequence correspond to lattices of comparable local structure, and thus it is possible to compare states for different values of  $\tau$ , for instance by comparing their reduced density matrix for one lattice site. The coarse-graining transformation can be understood as a real space renormalization group (RG) transformation and the sequence of e.g. reduced density matrices defines a RG flow. In the limit of an infinite lattice, and when  $|\Psi\rangle$  is the ground state of a quantum critical system, this RG flow is numerically seen to converge to a fixed point [1, 4].

The real space RG transformation on MERA states has a remarkable feature, shared with the RG transformation on MPS states discussed in [15], namely that it is *reversible*. Indeed, the state  $|\Psi_{\tau-1}\rangle$  can be fully recovered from its coarse-grained version  $|\Psi_\tau\rangle$  and the isometric transformation  $U^{[\tau]}$ . In other words, local information about the system is not lost along the RG flow, but simply decoupled from the system and stored in the disentanglers and isometries of  $U^{[\tau]}$ . We notice that this feature stems from the fact that the pure state  $|\Psi_{\tau-1}\rangle$  is coarse-grained into another state  $|\Psi_\tau\rangle$  that is still pure. This is clearly non-trivial. The coarse-graining transformation involves tracing out degrees of freedom corresponding to short length scales. In the likely event that some of these degrees of freedom are entangled with the rest, the resulting coarse-grained state will inevitably be

*mixed*. In other words, in order to obtain a sequence of pure states  $\{|\Psi_0\rangle, |\Psi_1\rangle, |\Psi_2\rangle, \dots\}$ , only local degrees of freedom (that is, tensor product factor spaces) that are unentangled with the rest of the Hilbert space can be safely traced out.

This last observation has an important implication. As larger scales are considered, more and more local degrees of freedom happen to be entangled. As a result, the RG transformation of [15] can only efficiently consider non-critical ground states in one spatial dimension. Instead, by using disentanglers, some of the locally entangled degrees of freedom become disentangled and can thus safely trace out, as we discussed in sect. II. The net result is that not only critical ground states in a one-dimensional lattice [1, 4], but also two-dimensional (critical or non-critical) ground states [4] can be addressed with the present approach, provided that an area law for entanglement [10] is observed in the latter case.

### B. Obtaining a MERA from another tensor network representation

We assume that we are provided with an efficient representation of  $|\Psi\rangle$  in terms of a tensor network. For instance, for a lattice  $\mathcal{L}$  in  $D = 1$  spatial dimensions,  $|\Psi\rangle$  may be provided with a MPS or a tree tensor network, whereas in  $D = 2$  spatial dimensions it may be provided with a PEPS. The special case where  $|\Psi\rangle$  is given in terms of a MERA on which a gate has been applied between two consecutive sites is of particular importance in the context of simulating time evolution, and will be dealt with in sect. ??.

Our goal is to produce a MERA  $U \in \mathcal{M}$  for  $|\Psi\rangle$  from the existing tensor network representation, that corresponds to a matrix  $W$ . We want to approximate  $W$  with  $U \in \mathcal{M}$  resulting from optimizing the expression

$$\max_{U \in \mathcal{M}} |\text{tr}(W^\dagger U)| = \max_{U \in \mathcal{M}} |W^\dagger U|, \quad (44)$$

where the trace can be removed because  $|\Psi\rangle$  is a pure state and therefore  $W$  and  $U$  are matrices with just one column—that is, they are column vectors, see Fig. (25).

This is an optimization of type CL, see Eq. (12). One way to address it is by replacing it with a sequence of alternating UL optimizations, one for each disentangler  $u$  and isometry  $w$  in the MERA, and to repeat the sequence until the cost function  $f(U) = |W^\dagger U|$  has converged. As in section IV, we find that a particularly convenient way to organize an alternating strategy consists in optimizing the MERA layer by layer. In this manner the causal structure of the MERA can be best exploited to minimize computational costs, the results are very robust, and the scheme can be modified to address systems with translational invariance with a cost logarithmic in the system size.

In the rest of this section, and for simplicity, we specialize to the case where  $\mathcal{L}$  is in one spatial dimension and  $W$  corresponds to a MPS.

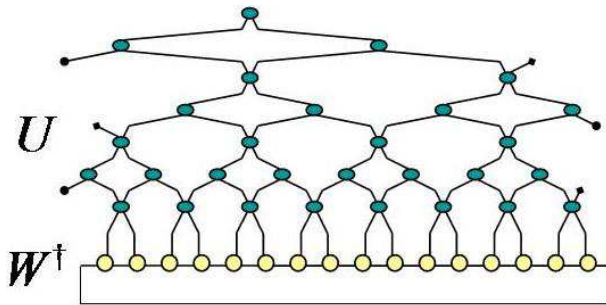


FIG. 25: Tensor network representation of the cost function  $|\text{tr}(W^\dagger U)|$  for the optimization over  $U \in \mathcal{M}$  in Eq. (44). Notice that  $W$ , representing the state  $|\Psi\rangle$  for which we want to obtain a MERA, is an MPS.

### C. Layered optimization

We replace the optimization (44) with a series of optimizations, each one involving just one layer of the MERA, corresponding to a length scale  $\lambda = 2^\tau$ . We distinguish between an initialization stage that runs from small to large length scales only once; and a convergence stages that sweeps over length scales, from large to small and back to large, several times until convergence of the cost function is achieved.

*Initialization stage.*— We initialize the MERA by performing a series of SCQ optimizations of the form

$$\max_{U^{[\tau]} \in \mathcal{M}^{[\tau]}} \text{tr}(U^{[\tau]\dagger} W_{\tau-1} W_{\tau-1}^\dagger U^{[\tau]}), \quad (45)$$

where  $W_\tau$  is an effective MPS and  $U^{[\tau]} \in \mathcal{M}^{[\tau]}$  is restricted by the circuit structure  $\mathcal{M}^{[\tau]}$ , made of one row of disentanglers and one row of isometries, see Fig. (26).

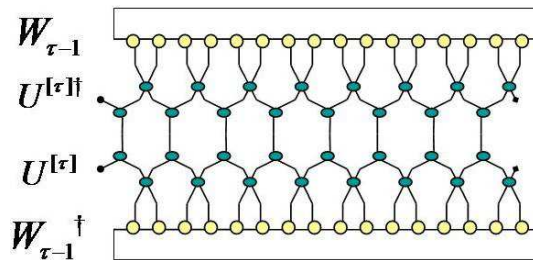


FIG. 26: Cost function for the SCQ optimization (45).

The initialization stage works by addressing the MERA layer by layer, from short length scales to large length scales. Starting with  $\tau = 1$ , we repeat the following two steps for increasing values of  $\tau$ ,  $1 \leq \tau \leq T - 1$ .

- E1. Given the MPS  $W_{\tau-1}$  for the state  $|\Psi_{\tau-1}\rangle$ , obtain the isometric transformation  $U^{[\tau]}$  according to optimization (45).
- E2. Given the MPS  $W_{\tau-1}$  and  $U^{[\tau]}$ , construct an effective MPS  $W_\tau$  for the state  $|\Psi_\tau\rangle$ .

Thus, iteration over  $\tau$  produces a sequence of MPS representations  $W_\tau$  and isometric transformations  $U^{[\tau]}$ ,

$$W_0 \rightarrow U^{[1]} \rightarrow W_1 \rightarrow U^{[2]} \rightarrow W_2 \rightarrow \dots \rightarrow W_{T-1} \rightarrow U^{[T]}. \quad (46)$$

The MERA is thus initialized to  $U \in \mathcal{M}$  as  $U = U^{[1]}U^{[2]} \dots U^{[T]}$ , where the top isometric transformation  $U^{[T]}$  has rank one and represents a pure state  $|\Psi_{T-1}\rangle$  of the two-site lattice  $\mathcal{L}_{T-1}$ .

*Convergence stage.*— The MERA can now be further improved. For each value of  $\tau$ , we consider the CL optimization

$$\begin{aligned} \max_{U^{[\tau]} \in \mathcal{M}^\tau} \text{tr}(W_{\tau-1}^\dagger U^{[\tau]} U^{[\tau+1]} \dots U^{[T]}) \\ = \max_{U^{[\tau]} \in \mathcal{M}^\tau} \text{tr}(W_{\tau-1}^\dagger U^{[\tau]} \tilde{W}_\tau), \end{aligned} \quad (47)$$

where  $\tilde{W}_\tau$  is a MPS that approximates the effective state  $|\tilde{\Psi}_\tau\rangle$  given by  $U^{[\tau+1]} \dots U^{[T]}$ . Notice that the CL optimization (47) takes into account both all the updated upper layers of the MERA,  $\{U^{[\tau+1]}, \dots, U^{[T]}\}$ , encoded in the MPS  $\tilde{W}_\tau$ , and all the updated lower layers of the MERA,  $\{U^{[1]}, \dots, U^{[\tau-1]}\}$ , that are encoded in the MPS  $W_{\tau-1}$ .

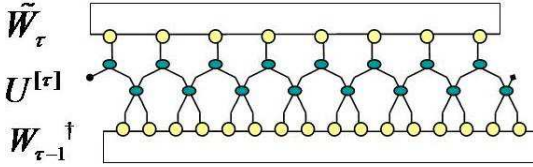


FIG. 27: Cost function for the CL optimization (47).

This part of the algorithm works by sweeping over all layers of the MERA, starting with the top layer ( $\tau = T$ ), then descending layer by layer to the lowest one  $\tau = 1$ , then ascending back to the top. The sweeping is repeated until the cost function converges. During the descent, the two following steps are performed for each value of  $\tau$ :

F1. Given  $\tilde{W}_\tau$  and  $W_{\tau-1}$ , compute  $U^{[\tau]}$  according to optimization (47).

F2. Given  $\tilde{W}_\tau$  and the updated  $U^{[\tau]}$ , compute an updated  $\tilde{W}_{\tau-1}$ .

During the ascent, the two steps to be performed for each value of  $\tau$  are the following:

G1. Given  $\tilde{W}_\tau$  and  $W_{\tau-1}$ , compute  $U^{[\tau]}$  according to optimization (47).

G2. Given  $W_{\tau-1}$  and the updated  $U^{[\tau]}$ , compute an updated  $W_\tau$ .

The computation of  $W_\tau$  and  $\tilde{W}_\tau$  in steps E2, F2 and G2 is illustrated in Fig. (28).

We note that whereas the convergence stage can be used to improve the MERA, the initialization process alone often produces already a good approximation to the original state, and therefore it may be all that is required in some applications.

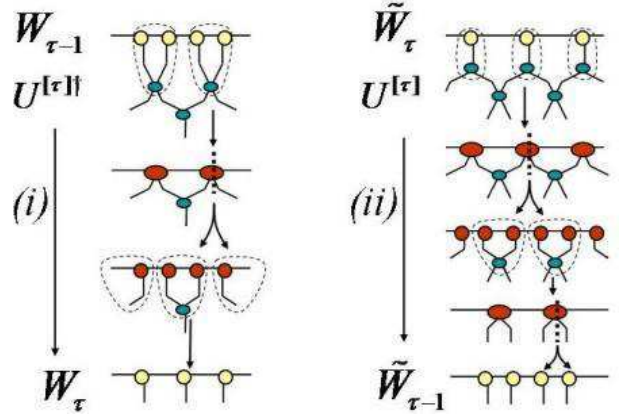


FIG. 28: (i) Computation of an MPS for  $W_\tau = U^{[\tau]\dagger} W_{\tau-1}$  from an MPS for  $W_{\tau-1}$  and a quantum circuit representation for  $U^{[\tau]}$ , as used in steps E2 and G2. (ii) Computation of an MPS for  $\tilde{W}_{\tau-1} = U^{[\tau]} \tilde{W}_\tau$  from an MPS for  $\tilde{W}_\tau$  and a quantum circuit representation for  $U^{[\tau]}$ , as used in step G1. Both computations can be achieved by using matrix multiplications (to turn several tensors into one) and singular value decompositions (to split a tensor into two).

#### D. Optimization of one layer: standard approach

Now we explain how to perform optimizations (45) and (47) for one layer of the MERA during the initialization and convergence stages.

We consider first the SCQ optimization of  $U^{[\tau]}$  during the initialization stage, Eq. (45). Following the linearization strategy outlined in Fig. (17), we replace this SCQ optimization with a CL optimization. In order to do this, we need to compute an auxiliary isometric transformation  $\tilde{W}_\tau$  (corresponding to  $x$  in Fig. (17)). This is done in step H0 below. Then the resulting CL optimization for  $U^{[\tau]}$  is of the form (47). We address it by performing repeated horizontal sweeps over the entire layer. For instance, a possible elementary round (to be repeated until convergence of the cost function) consists of the following steps:

H0. Compute an effective MPS  $\tilde{W}_\tau$  using  $U^{[\tau]}$  and the MPS  $W_{\tau-1}$ .

H1. Given  $\tilde{W}_\tau$ ,  $W_{\tau-1}$  and  $U^{[\tau]}$ , starting with  $s = 1$  and progressing for all possible odd values of  $s$ ,  $s = 1, 3, 5, \dots$ , update the disentangler  $u^{[\tau, s]}$  by means of a UL optimization. See Fig. (29).

H2. Given  $\tilde{W}_\tau$ ,  $W_{\tau-1}$  and  $U^{[\tau]}$ , starting with  $s = 1$  and progressing for all possible odd values of  $s$ ,  $s = 1, 3, 5, \dots$ , update the isometry  $w^{[\tau, s+1]}$  by means of a UL optimization. See Fig. (30).

Step H0 is identical to step G2 in the ascent phase of the convergence stage described above.

Finally, the optimization of  $U^{[\tau]}$  during the convergence stage, Eq. (47), is identical to steps H1-H2 for the

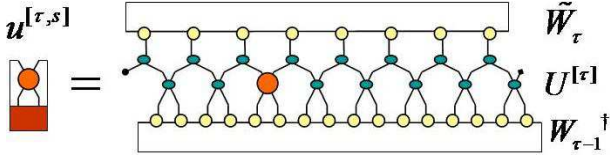


FIG. 29: Cost function  $|\text{tr}(W^\dagger u^{[\tau,s]})|$  in Eq. (11) for the optimization of disentangler  $u^{[\tau,s]}$  in step H1. This UL optimization can be addressed exactly, see Sect. III C.

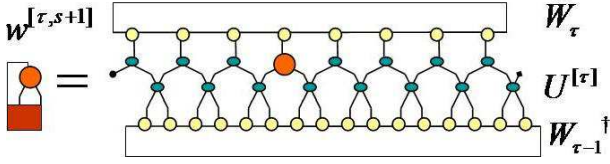


FIG. 30: Cost function  $|\text{tr}(W^\dagger w^{[\tau,s+1]})|$  in Eq. (11) for the optimization of disentangler  $w^{[\tau,s+1]}$  in step H2. This UL optimization can be addressed exactly, see Sect. III C.

initialization stage, but by using the  $\tilde{W}_\tau$  computed in step F2 instead of step H0.

### E. Optimization of one layer (II): local approach

Here we include an alternative approach to optimizing one layer of the MERA, Eqs. (45) and (47), by considering only local information about the state, namely reduced density matrices for a small number of neighboring sites.

We stress that, in contrast with the optimization in Sect. IV involving a local Hamiltonian (where the cost function for one layer naturally decomposes into pieces) here we *approximate* the global cost function with a collection of local cost functions. In doing so, we partially ignore, in optimizing a given tensor (a disentangler or an isometry), the changes sustained by distant tensors of the MERA. This comes at a price—the resulting MERA might be a less accurate description of the state  $|\Psi\rangle$ —but it makes computations more efficient in certain cases. This method does not require having a description of the whole state  $|\Psi_\tau\rangle$  at a given layer  $\tau$ , but just some of its reduced density matrices. It will be used in the hybrid algorithm described in Sect. VI.

We start by considering the optimization of the isometric transformation  $U^{[\tau]}$  during the initialization stage, Eq. (45), which we break into individual optimizations for the disentanglers  $u^{[\tau,s]}$  and isometries  $w^{[\tau,s+1]}$ . The optimization over the disentangler  $u^{[\tau,s]}$ , acting on sites  $[s, s+1] \in \mathcal{L}_{\tau-1}$ , is performed now by taking into consideration only a subset of neighboring tensors in the MERA. A minimal meaningful choice for this subset seems to be the disentanglers  $u^{[\tau,s-2]}$  and  $u^{[\tau,s+2]}$  and the isometries  $w^{[\tau,s-1]}$  and  $w^{[\tau,s+1]}$ , which form the immediate environment of  $u^{[\tau,s]}$  in  $U^{[\tau]}$ . We define the isometric transformation  $X^{[\tau,s]}$  acting on the 6-site block

$[s-2, \dots, s+3] \in \mathcal{L}_{\tau-1}$  as

$$X^{[\tau,s]} \equiv (w^{[\tau,s-1]} w^{[\tau,s+1]})(u^{[\tau,s-2]} u^{[\tau,s]} u^{[\tau,s+2]}), \quad (48)$$

and consider the 6-site reduced density matrix  $\pi_{\tau-1}^{[s]}$  of  $|\Psi_{\tau-1}\rangle$  on the same block. Then, see Figs. (31), (33) and (34),  $u^{[\tau,s]}$  is updated according to the UQ optimization

$$\max_{u^{[\tau,s]}} \text{tr}(X^{[\tau,s]} \pi_{\tau-1}^{[s]} X^{[\tau,s]\dagger}). \quad (49)$$

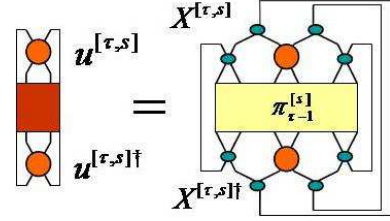


FIG. 31: Cost function  $\mathbf{x}^\dagger K \mathbf{x} = \sum_i \text{tr}(u^{[\tau,s]\dagger} M_i u^{[\tau,s]} N_i)$  in Eq. (13) for the optimization of disentangler  $u^{[\tau,s]}$  in Eq. (49). This UQ optimization can be addressed using the strategies described in Sect. III E. Alternatively, it can be replaced with a UL optimization, see Figs. (33) and (34).

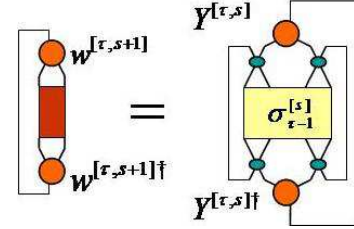


FIG. 32: Cost function  $\mathbf{x}^\dagger K \mathbf{x} = \text{tr}(w^{[\tau,s+1]\dagger} M w^{[\tau,s+1]})$  in Eq. (14) for the optimization of isometry  $w^{[\tau,s+1]}$ . This SUQ optimization can be addressed exactly, see Sect. III D.

The optimization over the isometry  $w^{[\tau,s+1]}$ , acting on sites  $[s+1, s+2] \in \mathcal{L}_{\tau-1}$ , is performed similarly by considering only the disentanglers  $u^{[\tau,s]}$  and  $u^{[\tau,s+2]}$ . We define the isometric transformation  $Y^{[\tau,s]}$  acting on the 4-site block  $[s, \dots, s+3] \in \mathcal{L}_{\tau-1}$  as

$$Y^{[\tau,s]} \equiv w^{[\tau,s+1]}(u^{[\tau,s]} u^{[\tau,s+2]}), \quad (50)$$

and consider the 4-site reduced density matrix  $\sigma_{\tau-1}^{[s]}$  of  $|\Psi_{\tau-1}\rangle$  on the same block. Then, see Fig. (32),  $w^{[\tau,s+1]}$  is updated according to the optimization

$$\max_{w^{[\tau,s+1]}} \text{tr}(Y^{[\tau,s]} \sigma_{\tau-1}^{[s]} Y^{[\tau,s]\dagger}). \quad (51)$$

The optimization of  $U^{[\tau]}$  in Eq. (45) is now achieved by repeatedly sweeping over the entire layer. For instance, a possible elementary round (to be repeated until convergence of the cost function) consists of the following steps:

- I1. Starting with  $s = 1$  and progressing for all possible odd values of  $s$ ,  $s = 1, 3, 5, \dots$ , update each disentangler  $u^{[\tau,s]}$  by means of the UQ optimization (49).
- I2. Starting with  $s = 1$  and progressing for all possible odd values of  $s$ ,  $s = 1, 3, 5, \dots$ , update the isometry  $w^{[\tau,s+1]}$  by means of a SUQ optimization (51).

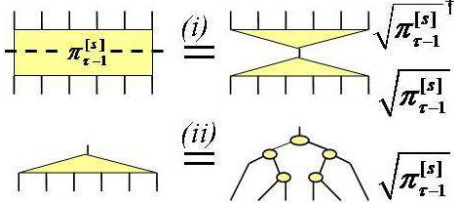


FIG. 33: (i) By means of an eigenvalue decomposition the density matrix  $\pi_{\tau-1}^{[s]}$  is purified into an operator  $(\pi_{\tau-1}^{[s]})^{1/2}$ , where  $\pi_{\tau-1}^{[s]} = (\pi_{\tau-1}^{[s]})^{1/2}(\pi_{\tau-1}^{[s]})^{1/2\dagger}$ . (ii) Tree tensor network representation of  $(\pi_{\tau-1}^{[s]})^{1/2}$ .

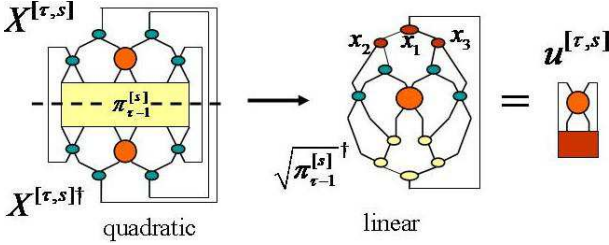


FIG. 34: Linearization of the cost function for the UQ optimization (49). The linearization is done by following steps similar to those in Fig. (17). It uses a tree tensor network representation of the purification  $(\pi_{\tau-1}^{[s]})^{1/2}$  of  $\pi_{\tau-1}^{[s]}$  described in Fig. (S5F9StatePurify), as well as three auxiliary tensors  $x_1$ ,  $x_2$  and  $x_3$ . Here  $x_1$  is a generic tensor whereas  $x_2$  and  $x_3$  are isometric tensors. An alternating sequence of UL optimizations is used to determine  $u^{\tau,s}$ ,  $x_1$ ,  $x_2$  and  $x_3$ .

The optimization of  $U^{[\tau]}$  during the convergence stage, Eq. (47), is very similar to the initialization, but with Eqs. (49) and (51) replaced with

$$\max_{u^{[\tau,s]}} \text{tr}(X^{[\tau,s]} \pi_{\tau-1}^{[s]} X^{[\tau,s]\dagger} \tilde{\pi}_{\tau}^{[s]}). \quad (52)$$

and

$$\max_{w^{[\tau,s+1]}} \text{tr}(Y^{[\tau,s]} \sigma_{\tau-1}^{[s]} Y^{[\tau,s]\dagger} \tilde{\sigma}_{\tau}^{[s]}). \quad (53)$$

where  $\tilde{\pi}_{\tau}^{[s]}$  and  $\tilde{\sigma}_{\tau}^{[s]}$  are a two-site and one-site reduced density matrices on lattice  $\mathcal{L}_{\tau}$  that minimally account for the MERA on upper layers. The optimization of  $U^{[\tau]}$  proceeds as in the initialization stage, according to two steps analogous to steps I1 and I2.

## F. Computational cost

As in the previous section, the optimization of the isometric transformation  $U^{[\tau]}$  requires a number of operations proportional to the number of sites in  $\mathcal{L}_{\tau}$ . The MERA has only  $O(N)$  tensors and the cost of optimizing all of them (e.g. in the initialization stage or in one round of the convergence stage) scales as  $O(N\chi^p\chi_{MPS}^q)$ , where  $\chi_{MPS}$  labels the rank of the MPS  $W$ , and  $p$  and  $q$  are small integers that depend on several factors, including whether we use the standard approach or the local approach to optimize one layer of the MERA, and whether the ends of the MPS are closed or open (to describe states in a system with periodic or open boundary conditions).

Important additional computational gains can be obtained in the case that  $|\Psi\rangle$  is a state invariant under translations in a system with periodic boundary conditions. There we can enforce the MERA itself to be invariant under translations, e.g. by requiring that all the disentanglers and isometries in a layer be the same. In that case, only a constant number of tensors need to be optimized in each layer, at a constant computational cost, so that the overall cost of obtaining a MERA from an MPS is lowered from  $O(N)$  to just  $O(\log N)$ . In particular, the MPS of an infinite system (open or periodic boundary conditions) can be translated into a MERA of  $\tau$  layers at a cost  $O(\tau)$ . This strategy was used in the first exploratory calculations of renormalized entanglement in Ref. [1], where blocks of several thousands of spins could be considered. It is also the basis of several results in [4] involving infinite systems in both one and two spatial dimensions.

## VI. HYBRID ALGORITHM

In this section we describe an algorithm to compute a MERA for certain target states. Given a local Hamiltonian  $H$ , possible target states are its ground state  $|\Psi_{gr}\rangle$  and low energy excited states.

The hybrid algorithm is based on mixing the strategies already discussed in Sects. IV and V. It requires, in addition, the use of an *auxiliary algorithm*, such as DMRG [2], TEBD [16] and variational MPS [13] for systems in  $D = 1$  spatial dimensions or PEPS [9] for the  $D = 2$  case. Thus, this algorithm combines the power of other well-established methods with the scalability offered by entanglement renormalization.

For simplicity, we consider a system in  $D = 1$  spatial dimensions only. A generalization of this algorithm to deal with systems in  $D > 1$  dimensions, using the  $D$ -dimensional MERA, is conceptually straightforward.

### A. Combining the MERA with other algorithms

We consider a many-body system characterized by a lattice  $\mathcal{L}$  in  $D = 1$  spatial dimensions made of  $N$  sites

( $N = 2^T$  for some integer  $T$ ) and a local Hamiltonian  $H : \mathbb{V}^{\otimes N} \rightarrow V^{\otimes N}$  that decomposes as a sum of local terms as in Eq. (34). Our goal is to obtain a MERA representation for some *target* state  $|\Psi\rangle \in \mathbb{V}^{\otimes N}$ , to be further specified below, from knowledge of  $H$  and with the help of an auxiliary algorithm.

As in previous sections, we consider a sequence of increasingly coarse-grained lattices  $\{\mathcal{L}_0, \mathcal{L}_1, \dots, \mathcal{L}_{T-1}\}$ , where  $\mathcal{L}_0 \equiv \mathcal{L}$  is the original lattice and  $\mathcal{L}_\tau$  is associated with length scale  $\lambda_\tau = 2^\tau$ . We also consider a sequence of corresponding effective Hamiltonians  $\{H_0, H_1, \dots, H_{T-1}\}$  and states  $\{|\Psi_0\rangle, |\Psi_1\rangle, \dots, |\Psi_{T-1}\rangle\}$ , where  $H_0 \equiv H$  and  $|\Psi_0\rangle \equiv |\Psi\rangle$  are the original Hamiltonian and target state.

Given a local Hamiltonian  $H_\tau$ , the hybrid algorithm assumes the ability to compute  $|\Psi_\tau\rangle$ . This can be achieved with some auxiliary algorithm. We distinguish two possibilities: (i) The whole target state  $|\Psi_\tau\rangle$  is computed, for instance in the form of an MPS (or a PEPS in  $D = 2$ ); (ii) only local reduced density matrices for  $|\Psi_\tau\rangle$  are computed (specifically, the reduced density matrix  $\pi_\tau^{[s]}$  for a block of six contiguous sites  $[s-2, \dots, s+3] \in \mathcal{L}_\tau$  and the reduced density matrix  $\sigma_\tau^{[s]}$  for a block of four contiguous sites  $[s-1, \dots, s+2] \in \mathcal{L}_\tau$ , for  $s = 1, 3, 5, \dots$ ). In the first and second cases above, we say the auxiliary algorithm computes  $|\Psi_\tau\rangle$  *globally* and *locally* respectively.

## B. Computation of ground states

We address first the case where the target state  $|\Psi\rangle$  is the ground state  $|\Psi_{gr}\rangle$  of  $H$ . The hybrid algorithm builds a MERA by progressing over increasingly large length scales. Starting with  $\tau = 1$ , we repeat the following three steps for increasing values of  $\tau$ ,  $1 \leq \tau \leq T - 1$ .

- J1. Given Hamiltonian  $H_{\tau-1}$  for lattice  $\mathcal{L}_{\tau-1}$ , compute the ground state  $|\Psi_{\tau-1}\rangle$ .
- J2. Given  $|\Psi_{\tau-1}\rangle$ , compute the isometric transformation  $U^{[\tau]}$ .
- J3. Given  $H_{\tau-1}$  and  $U^{[\tau]}$ , construct a local Hamiltonian  $H_\tau$  for  $\mathcal{L}_\tau$ .

Thus, iteration over  $\tau$  produces a sequence of states, isometric transformations and effective Hamiltonians,

$$H_0 \rightarrow |\Psi_0\rangle \rightarrow U^{[1]} \rightarrow H_1 \rightarrow |\Psi_1\rangle \rightarrow \dots \rightarrow U^{[T]}. \quad (54)$$

The MERA  $U \in \mathcal{M}$  for the ground state corresponds to  $U = U^{[1]}U^{[2]} \dots U^{[T]}$ , where the top  $U^{[T]}$  has rank one and represents a pure state  $|\Psi_{\tau-1}\rangle$  of the two-site lattice  $\mathcal{L}_{\tau-1}$ .

The steps J1-J3 above are addressed as follows. In step J1, the auxiliary algorithm is used to compute  $|\Psi_{\tau-1}\rangle$  either globally (that is, producing an MPS representation  $W_{\tau-1}$ ) or locally (producing reduced density matrices  $\pi_{\tau-1}^{[s]}$  and  $\sigma_{\tau-1}^{[s]}$  for  $s = 1, 3, 5, \dots$ ) [19]. Step J2

is achieved with the techniques for optimizing one layer (initialization stage) discussed in Sect. V. In particular, we can use steps H0-H2 of the standard approach of sect. VD for a global computation, and steps I1-I2 of the local approach of Sect. VE for a local computation. Finally, step J3 is identical to step A2 in sect. IV.

## C. Computation of excitations

Let us now consider the case where the target state  $|\Psi\rangle$  is a low energy excitation of a local Hamiltonian  $H$  invariant under translations by one lattice site. We consider both finite systems (periodic boundary conditions) and infinite systems (open or periodic boundary conditions). For every relevant value of the momentum  $k$ , we consider the excited state  $|\Psi(k)\rangle$  above the ground state  $|\Psi_{gr}\rangle$ ,

$$\langle \Psi_{gr} | \Psi(k) \rangle = 0, \quad (55)$$

with well-defined momentum  $k$

$$T|\Psi(k)\rangle = e^{-ik}|\Psi(k)\rangle \quad (56)$$

and energy  $\epsilon(k)$ ,

$$H|\Psi(k)\rangle = \epsilon(k)|\Psi(k)\rangle, \quad (57)$$

where for simplicity we assume that  $\epsilon(k)$  is as small as possible (lowest energy branch of excitations).

The proceed essentially as in the case where the target is the ground state  $|\Psi_{gr}\rangle$ , by following steps J1-J3 with a local calculation of  $|\Psi\rangle$ . The main difference is that not only  $|\Psi(k)\rangle$  but also the ground state  $|\Psi_{gr}\rangle$  needs to be computed, and the MERA is built so as to represent both states simultaneously. The auxiliary algorithm to compute the reduced density matrices  $\pi$  and  $\sigma$  for the target state is discussed in [20].

## D. Computational cost

The hybrid algorithm computes the MERA with  $O(N\chi^p\chi_{MPS}^q)$  operations (see Sect. VF). To this cost, we need to add the cost incurred by the auxiliary algorithm, that in the algorithms listed in [19] is of the order  $O(N\chi_{MPS}^{q'})$  where  $q' = 3$  for open boundary conditions and  $q' = 5$  for periodic boundary conditions.

These costs can be reduced from  $O(N)$  to  $O(\log N)$  in a system that is invariant under translations, by using a translation invariant MERA, as we discussed in Sect. VF (the cost of each computation using the auxiliary algorithm can be brought to a constant [20]). In an infinite system, the first  $\tau$  layers of a MERA, characterizing the system up to a length scale  $\lambda_\tau = 2^\tau$ , can be computed with cost  $O(\tau)$ .

The hybrid algorithm requires the use of an auxiliary algorithm to compute the target state  $|\Psi\rangle$ . A natural

question is then whether the hybrid algorithm is needed at all. In order to clarify this point, we make two remarks. (i) We stress that the hybrid algorithm can work with just a local description of the target state  $|\Psi\rangle$  (in the form of reduced density matrices) and thus in principle it does not require computing  $|\Psi\rangle$  globally. (ii) The MPS representation underlying the DMRG [2], TEBD [16] and variational MPS [13] approaches (equivalently, the PEPS representation [9] in  $D = 2$  spatial dimensions) often leads to an excellent local description of  $|\Psi\rangle$ , but it is significantly less accurate at describing large scale properties, such as two-point correlators for large distances. The key advantage of the hybrid algorithm is that it recomputes the target state at each level of coarse-graining. This leads to a very precise description of correlations at large length scales, of interest e.g. in the study quantum phase transitions.

## VII. CONCLUSIONS

The MERA has been shown to be a good representation for the ground state of quantum many-body systems defined on a lattice in  $D \geq 1$  spatial dimensions and particularly suited to describe quantum phase transitions [1] and topological order [5]. Here we have described four algorithms, based on the MERA, to accomplish a series of tasks, including the computation of the ground state and low energy excitations of a local Hamiltonian  $H$  and the simulation of time evolution according to  $H$ . We envisage that these algorithms will facilitate the study of quantum criticality and emergent quantum many-body phenomena.

At the algorithmic level, one difficulty posed by the MERA is that it often requires solving a quadratic optimization over an isometric tensor (type UQ), which has no known analytical solution. In Sect. III we have proposed a number of strategies to perform such optimizations. Another difficulty is posed by the need to simultaneously optimize over many different isometric tensors. This has been addressed by using a sequence of alternating optimizations over individual tensors. Notice that special attention has been placed in organizing these sequences, which are implemented by sweeping the system both *vertically* (over different length scales) and *horizontally* (over different sites of a given effective lattice), where the characteristic causal structure of the MERA also plays an important role by minimizing the computational cost.

A major feature of the algorithms is that the cost of a simulation drops from  $O(N)$  to  $\log(N)$  in the case of a system that is invariant under translations. This is

due to the fact that the MERA is able to assimilate the symmetries of the system under study. In particular, in a critical system invariant under change of scale the tensors at different layers of the MERA can be chosen to be the same, leading to a very compact representation of the state in terms of  $O(N^0)$  parameters. Another way to significantly increase the efficiency of the description is, in the presence of internal symmetries such as particle number of conservation ( $U(1)$  symmetry) or spin isotropy ( $SU(2)$  symmetry), by adjusting the isometric tensors so as to retain only the degrees of freedom that are not fixed by the symmetry. Specific algorithms to incorporate scale invariance and internal symmetries in the simulations are considered in Refs. [4, 21].

Here we have detailed algorithms for the case of systems in  $D = 1$  spatial dimension only. The generalization to larger dimensions is conceptually straightforward, in that no additional ideas are required. This is due, in part, to the fact that the MERA seems to be a good representation of ground states also for  $D > 1$  [4]. However, the computations are markedly more resource intensive. In  $D > 1$  spatial dimensions a causal cone becomes stable when its intersection with an effective lattice  $\mathcal{L}_\tau$  contains a hypercube of  $3^D$  sites [3], and not just 3 sites as in the  $D = 1$  case. Thus, the cost of a computation scales as  $O(N\chi^{p_D})$ , where  $p_D$  is an integer roughly linear in  $D$ .

**Note:** After completion of all the results presented in this manuscript, we have learned of a related work. C. M. Dawson, J. Eisert and T. J. Osborne [22] have proposed an alternative approach to optimizing over quantum circuits, based on flow equation methods, that could be of significant interest as an alternative approach to optimizing the MERA. We also draw attention to Ref. [23], where M. Rizzi, S. Montangero and G. Vidal discuss an algorithm to update the MERA during a time evolution.

*Acknowledgements.* — Support from the Australian Research Council through a Federation Fellowship is acknowledged. The algorithms presented in these notes have been developed over several years, including a period (Summer 2003 to Summer 2005) when the author was at the Institute for Quantum Information at the California Institute of Technology, Pasadena, US. The use of steepest descend methods for the computation of disentanglers was investigated by Surjeet Rajendran during his Summer Research project in 2003 (Caltech SURF project, supervised by G.V.). Inspired in the ALS approach to variational MPS [13] and PEPS [9], steepest descend methods were later replaced with more efficient alternating methods. The author thanks Frank Verstraete for a crucial introduction to the ALS methods in MPS and PEPS and for key suggestions that lead to some of the optimization methods described in Sect. III.

---

[1] G. Vidal, arXiv:cond-mat/0512165v2

[2] S. R. White, Phys. Rev. Lett. **69**, 2863 (1992), Phys. Rev.

B **48**, 10345 (1993). U. Schollwoeck, Rev. Mod. Phys. **77**, 259 (2005).

- [3] G. Vidal, arXiv:quant-ph/0610099v1.
- [4] G. Evenbly et al, *in preparation*.
- [5] M. Aguado et al, *in preparation*.
- [6] I. Markov, Y.-Y. Shi, arXiv:quant-ph/0511069.
- [7] M. Fannes, B. Nachtergaele and R. F. Werner, *Comm. Math. Phys.* **144**, 3 (1992), pp. 443-490. S. Östlund and S. Rommer, *Phys. Rev. Lett.* **75**, 19 (1995), pp. 3537. D. Perez-Garcia, F. Verstraete, M.M. Wolf, J.I. Cirac, arXiv:quant-ph/0608197.
- [8] Y.-Y. Shi, L.-M. Duan, G. Vidal, *Phys. Rev. A* **74**, 022320 (2006).
- [9] F. Verstraete, J. I. Cirac, arXiv:cond-mat/0407066. V. Murg, F. Verstraete, J. I. Cirac, arXiv:cond-mat/0611522.
- [10] M. Sredniicki, *Phys. Rev. Lett.* **71**, 666 (1993). G. Vidal, J.I. Latorre, E. Rico, A. Kitaev, *Phys. Rev. Lett.* **90**, 227902 (2003). M. Plenio, J. Eisert, J. Drieg, and M. Cramer, *Phys. Rev. Lett.* **94**, 060503 (2005).
- [11] In particular, the results of Sect. III can be used to optimize any tensor network representation, such as MPS and tree tensor networks, that can be rewritten as a quantum circuit.
- [12] [http://en.wikipedia.org/wiki/Singular\\_value\\_decomposition](http://en.wikipedia.org/wiki/Singular_value_decomposition)
- [13] F. Verstraete, D. Porras, J. I. Cirac, *Phys. Rev. Lett.* **93**, 227205 (2004). D. Porras, F. Verstraete, J. I. Cirac, arXiv:cond-mat/0504717
- [14] Simulations with a local Hamiltonian with long range interactions are also possible with the MERA. In this case, the relevant causal cone is the union of causal cone for all the sites connected by an interaction term.
- [15] F. Verstraete, J.I. Cirac, J.I. Latorre, E. Rico, M.M. Wolf, *Phys. Rev. Lett.* **94** (2005) 140601.
- [16] G. Vidal, *Phys. Rev. Lett.* **91**, 147902 (2003); *ibid.* *Phys. Rev. Lett.* **93**, 040502 (2004).
- [17] G. Vidal, *Phys. Rev. Lett.* **98**, 070201 (2007).
- [18] J. Jordan, R. Orus, G. Vidal, F. Verstraete, J. I. Cirac, arXiv:cond-mat/0703788
- [19] In step J1, an MPS for  $|\Psi_{\tau-1}\rangle$  can be computed using a number of algorithms, with simple variations to account for three-site interactions. For instance, the TEBD (imaginary time evolution) can be used for finite [16] and infinite [17] systems with open boundary conditions, whereas the techniques of [13, 20] can be used for systems with periodic boundary conditions. In a generalization to  $D = 2$  spatial dimensions, a PEPS for  $|\Psi_{\tau-1}\rangle$  can be computed with open boundary conditions, in a finite [9] and infinite system [18], and with periodic boundary conditions [20].
- [20] F. Verstraete et al. *in preparation*.
- [21] S. Sukhbindar et al, *in preparation*.
- [22] C. M. Dawson, J. Eisert, T. J. Osborne, arXiv:0705.3456.
- [23] M. Rizzi, S. Montangero, G. Vidal, arXiv:0706.0868 (accepted in PRA).